Electronic Supplementary Material (ESI) for Dalton Transactions.
This journal is © The Royal Society of Chemistry 2021

Precise control of the degree and regioselectivity of functionalization in nitro- and amino-functionalized di(trispyrazolylborato)iron(II) spin crossover complexes

Chenyang Ma, Claire Besson*

Department of Chemistry, The George Washington University, 800 22nd Street NW,

Washington, D.C. 20052, United States

SUPPLEMENTARY INFORMATION

Solid-state structure of all compounds

Solid-state structure of TBA[3-NO_2Tp]

a.) b.)

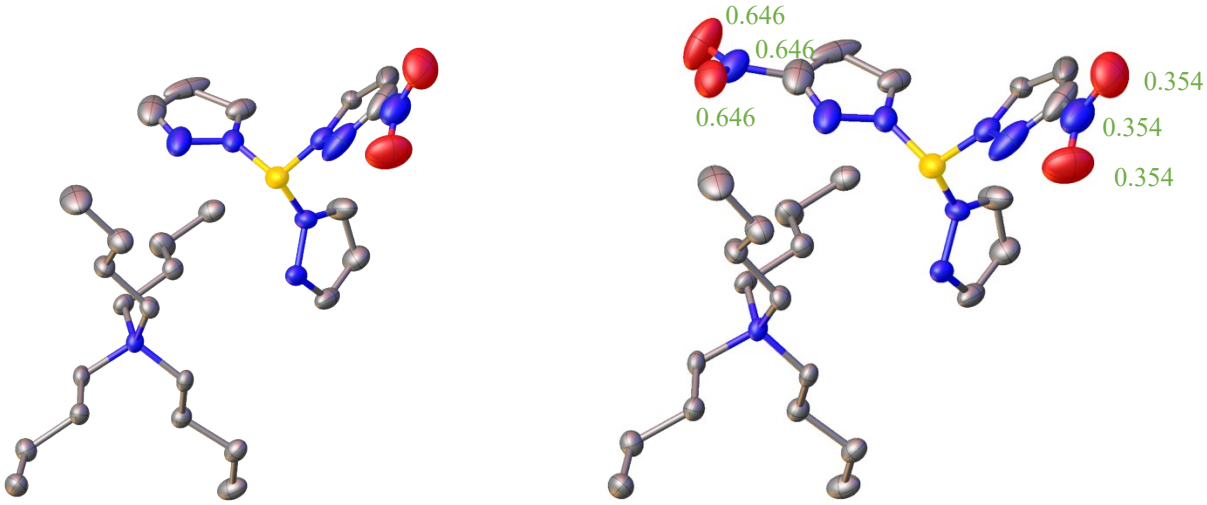

Figure 1. a). Solid-state structure of TBA[3-NO_2Tp] showing only the lowest occupancy component of the disorder. b) Asymmetric unit of ligand TBA [3-NO_2Tp] with indications of non-unit site occupancy. Thermal ellipsoids are shown at 50% probability. Color code: B, yellow; C, grey; N, blue; O, red. Hydrogen atoms are omitted for clarity.

Solid-state structure of TBA[4-NO_2Tp]

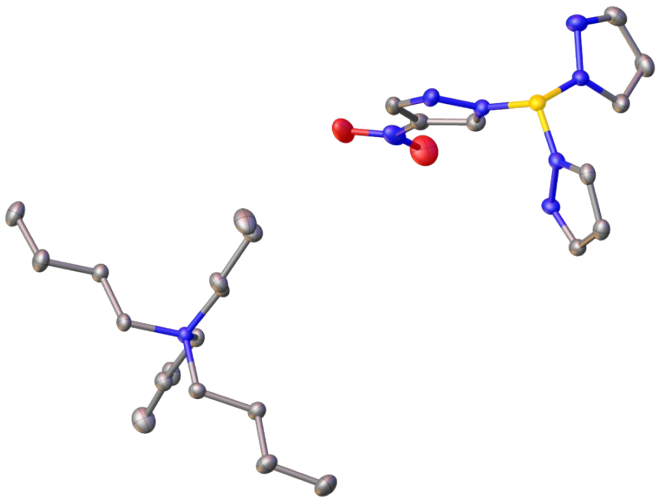

Figure 2. Solid-state structure of TBA[4-NO_2Tp]. Thermal ellipsoids are shown at 50% probability. Color code: B, yellow; C, grey; N, blue; O, red. Hydrogen atoms are omitted for clarity.

Solid-state structure of [(3-NO_2Tp)$_2$Fe]

a.) b.)

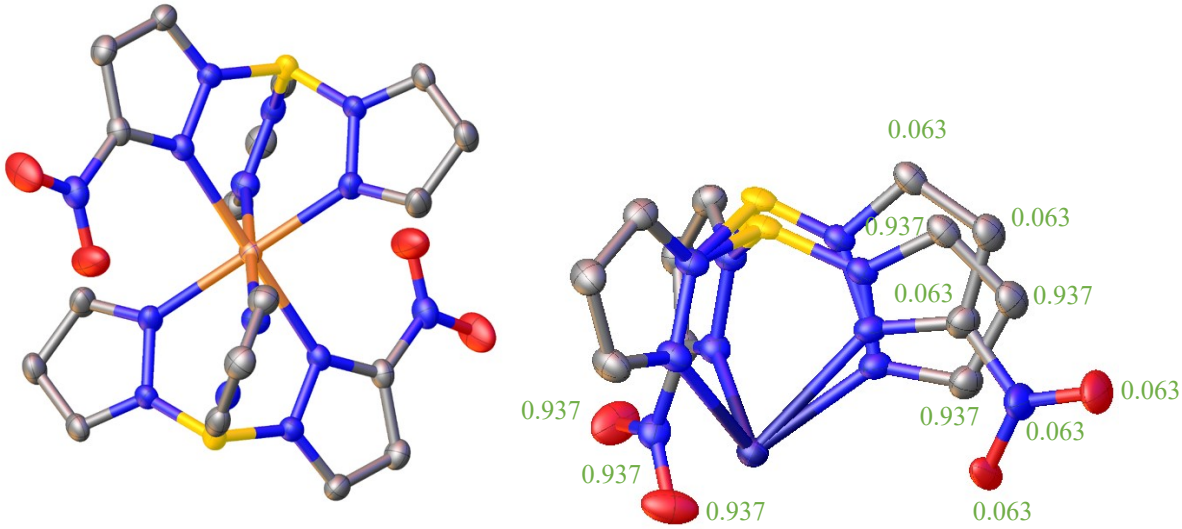

Figure 3. a). Solid-state structure of [(3-NO_2Tp)$_2$Fe], showing only the highest occupancy component of the disorder. b) Asymmetric unit of complex [(3-NO_2Tp)$_2$Fe], with indications of non-unit site occupancy. Thermal ellipsoids are shown at 50% probability. Color code: Fe, brown; B, yellow; C, grey; N, blue; O, red. Hydrogen atoms are omitted for clarity.

Solid-state structure of [(Tp)Fe(3-NO_2Tp)]$\cdot$ $(C_6H_6)_{0.5}$

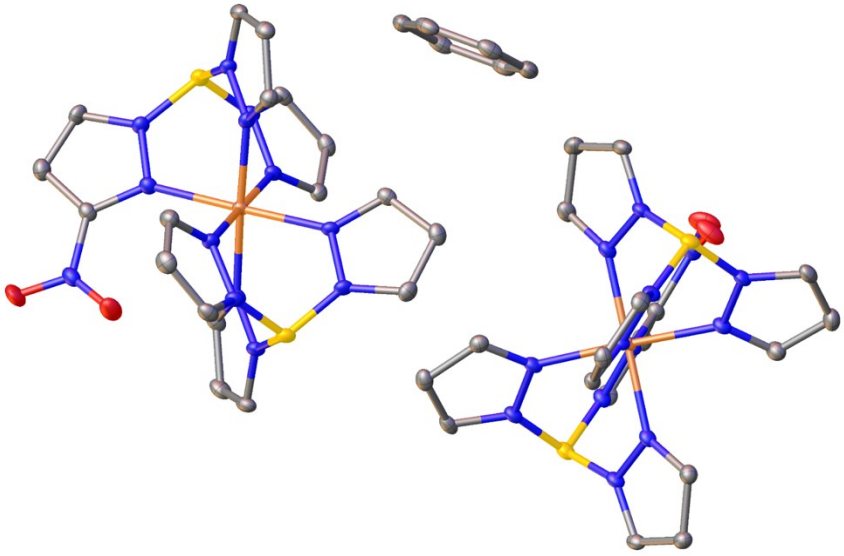

Figure 4. Solid-state structure of [(Tp)Fe(3-NO_2Tp)]$\cdot$ $(C_6H_6)_{0.5}$. Thermal ellipsoids are shown at 50% probability. Color code: Fe, brown; B, yellow; C, grey; N, blue; O, red. Hydrogen atoms are omitted for clarity.

Solid-state structure of [(Tp)Fe(4-NO_2Tp)]

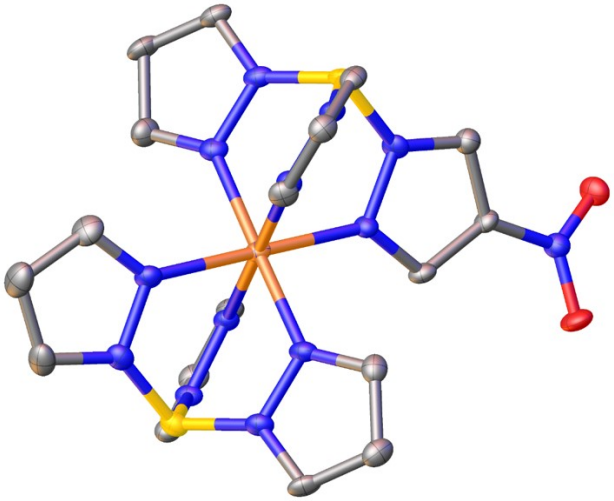

Figure 5. Solid-state structure of [(Tp)Fe(4-NO_2Tp)]. Thermal ellipsoids are shown at 50% probability. Color code: Fe, brown; B, yellow; C, grey; N, blue; O, red. Hydrogen atoms are omitted for clarity.

Solid-state structure of [(Tp)Fe(5-NO_2Tp)]· $(CH_3CN)_{0.5}$

a.) b.)

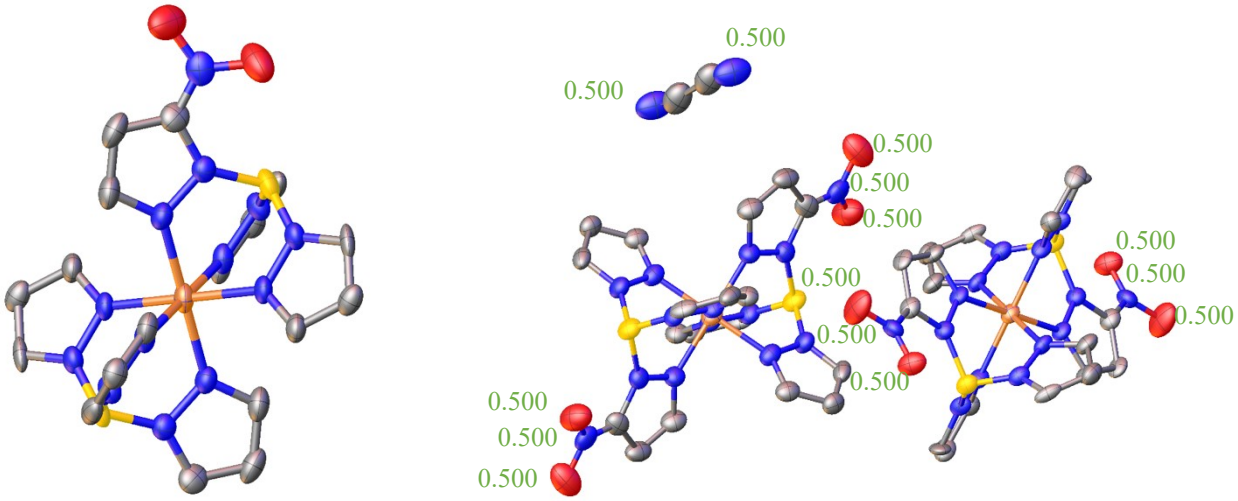

Figure 6. a). Solid-state structure of [(Tp)Fe(5-NO_2Tp)], showing only one component of the disorder. The co-crystallizing acetonitrile moiety is omitted for clarity. b) Solid-state structure of complex [(Tp)Fe(5-NO_2Tp)] · $(CH_3CN)_{0.5}$ with indications of non-unit site occupancy. Thermal ellipsoids are shown at 50% probability. Color code: Fe, brown; B, yellow; C, grey; N, blue; O, red. Hydrogen atoms are omitted for clarity.

Solid-state structure of [((3-NO_2)$_2$Tp)$_2$Fe]

a.) b.)

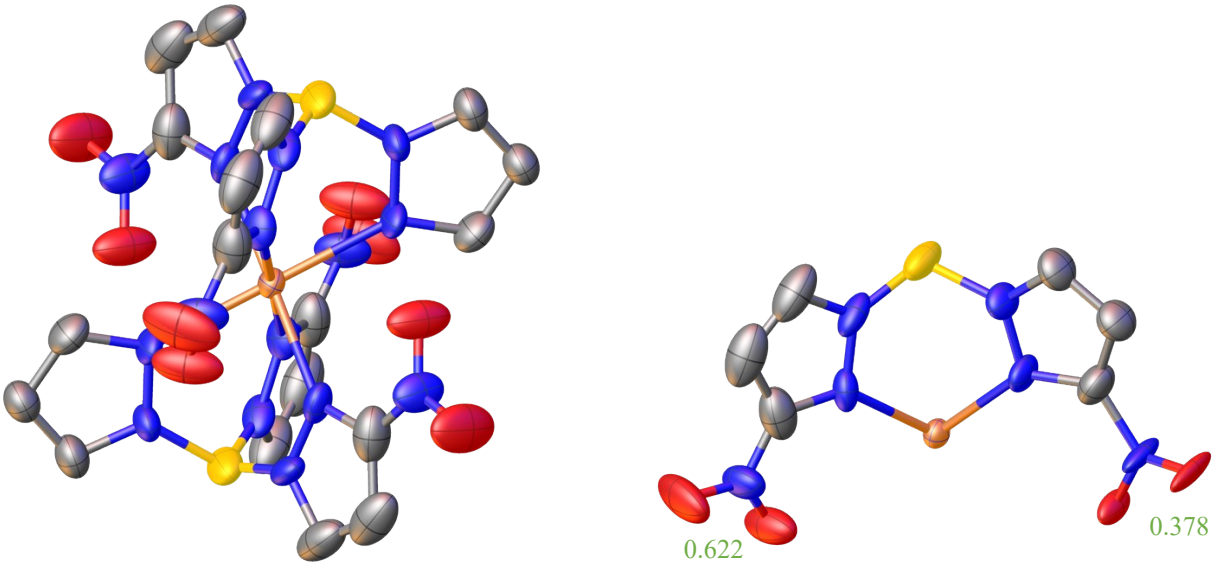

Figure 7. a). Solid-state structure of [((3-NO_2)$_2$Tp)$_2$Fe], showing only the highest occupancy component of the disorder. b) Asymmetric unit of complex [((3-NO_2)$_2$Tp)$_2$Fe], with indications of non-unit site occupancy. Thermal ellipsoids are shown at 50% probability. Color code: Fe, brown; B, yellow; C, grey; N, blue; O, red. Hydrogen atoms are omitted for clarity.

Solid-state structure of [((3-NO_2)$_2$Tp)$_2$Fe]·CH_2Cl_2

a.) b.)

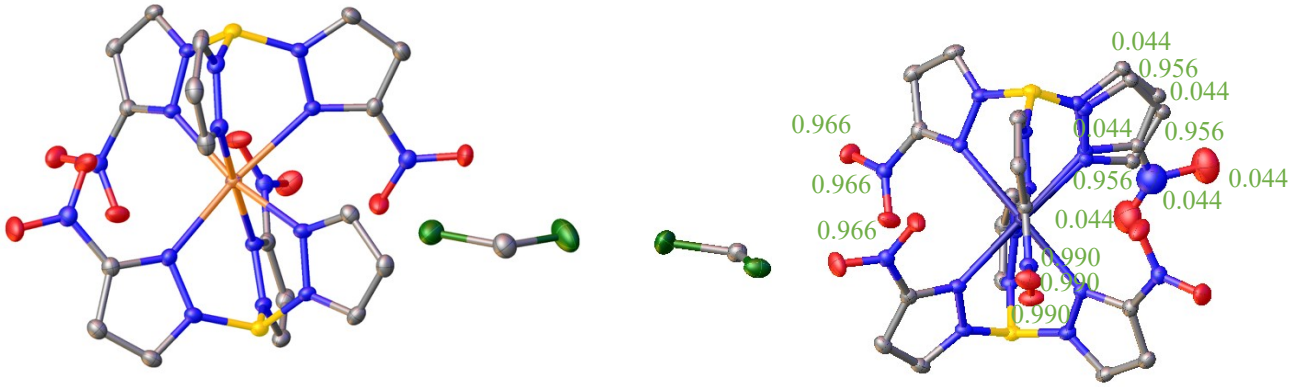

Figure 8. a). Solid-state structure of [((3-NO_2)$_2$Tp)$_2$Fe]·CH_2Cl_2, showing only the highest occupancy component of the disorder. b). Asymmetric unit of complex [((3-NO_2)$_2$Tp)$_2$Fe]·CH_2Cl_2, with indications of non-unit site occupancy. Thermal ellipsoids are shown at 50% probability. Color code: Fe, brown; B, yellow; C, grey; N, blue; O, red; Cl, green. Hydrogen atoms are omitted for clarity.

Solid-state structure of [(3-NH_2Tp)$_2$Fe]

a.) b.)

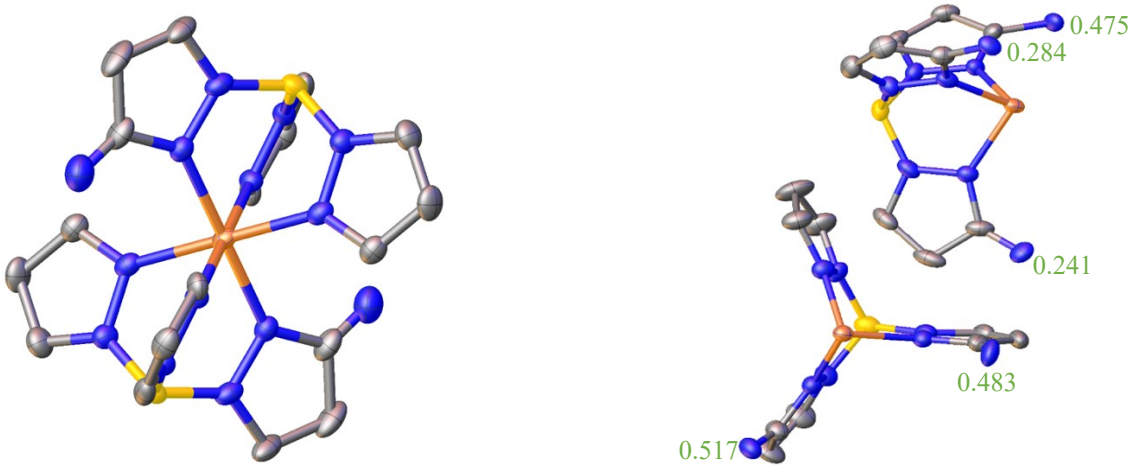

Figure 9. a). Solid-state structure of [(3-NH_2Tp)$_2$Fe], showing only the highest occupancy component of the disorder. b) Asymmetric unit of complex [(3-NH_2Tp)$_2$Fe] with indications of non-unit site occupancy. Thermal ellipsoids are shown at 50% probability. Color code: Fe, brown; B, yellow; C, grey; N, blue. Hydrogen atoms are omitted for clarity.

Solid-state structure of [((3-NH_2)$_2$Tp)$_2$Fe]

a.) b.)

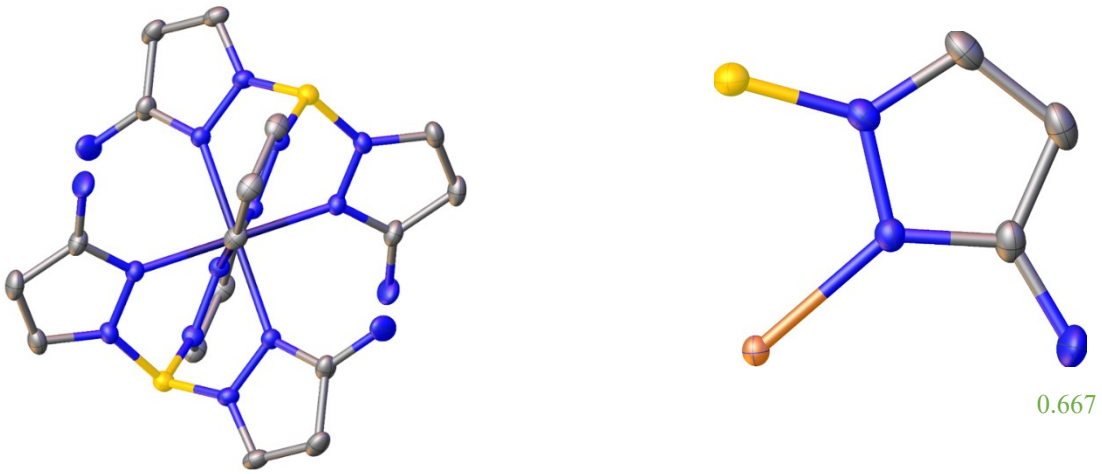

Figure 10. a). Solid-state structure of [((3-NH_2)$_2$Tp)$_2$Fe], ommiting the disorder. b) Asymmetric unit of complex [((3-NH_2)$_2$Tp)$_2$Fe] with an indication of non-unit site occupancy. Thermal ellipsoids are shown at 50% probability. Color code: Fe, brown; B, yellow; C, grey; N, blue. Hydrogen atoms are omitted for clarity.

X-ray crystallography

Table 1. Single-crystal X-ray diffraction analysis details of ligands

	TBA[3-NO_2Tp]	TBA[4-NO_2Tp]
CCDC number	2016677	2016678
Formula	$C_{25}H_{45}BN_8O_2$	$C_{25}H_{45}BN_8O_2$
Fw / g mol^{-1}	500.50	500.50
Crystal size / mm^3	0.31, 0.25, 0.12	0.71, 0.42, 0.24
crystal system	monoclinic	monoclinic
space group	$P2_1/n$	$P2_1/n$
a / Å	12.034(2)	9.9736(15)
b / Å	15.744(3)	14.258(2)
c / Å	14.929(3)	20.471(3)
α	90	90
β	95.216(4)	94.132(2)
γ	90	90
V / $Å^3$	2816.9(8)	2903.5(8)
Z	4	4
ρcalc / g cm^{-3}	1.178	1.145
μ / mm^{-1}	0.077	0.075
λ / Å	Mo Kα (0.71073)	Mo Kα (0.71073)
T / K	298(2)	100(2)
2θmax	51.6°	54.3°
reflections collected	17918	20405
independent reflections	4872	5101
parameters	358	330
R(int)	0.0461	0.0538
R1 [I > 2σ(I)]	0.0805	0.0449
wR2 (all data)	0.2305	0.1197
Largest peak and hole / e $Å^{-3}$	0.540, -0.456	0.242, -0.263

	[(3-NO_2Tp)$_2$Fe]	[(Tp)Fe(3-NO_2Tp)]	[(Tp)Fe(4-NO_2Tp)]	[(Tp)Fe(5-NO_2Tp)]	[(Tp)Fe(5-NO_2Tp)]	[((3-NO_2)$_2$Tp)$_2$Fe]

		$\cdot(C_6H_6)_{0.5}$		$\cdot(CH_3CN)_{0.5}$	$\cdot(CH_3CN)_{0.5}$	
CCDC number	2017277	2017280	2018041	2024174	2019476	2109964
Formula	$C_{18}H_{18}B_2FeN_{14}O_4$	$C_{21}H_{22}B_2FeN_{13}O_2$	$C_{18}H_{19}B_2FeN_{13}O_2$	$C_{38}H_{41}B_4Fe_2N_{27}O_4$	$C_{19}H_{20.5}B_2FeN_{13.5}O_2$	$C_{18}H_{16}B_2FeN_{16}O_8$
Fw / g mol^{-1}	571.93	565.98	526.93	1094.92	547.46	661.98
Crystal size / mm^3	0.13, 0.82, 0.58	0.15, 0.91, 0.17	0.066, 0.17, 0.291	0.12, 0.34, 0.15	0.16, 0.42, 0.07	0.20. 0.12, 0.07
crystal system	triclinic	monoclinic	monoclinic	monoclinic	monoclinic	orthorhombic
space group	*P*-1	$P2_1/c$	$P2_1/c$	$C2/c$	$C2/c$	*Cmce*
a / Å	7.4826(19)	7.6174(5)	7.5560(19)	15.695(3)	15.9020(13)	13.482(3)
b / Å	8.807(2)	16.9017(11)	18.433(5)	17.914(4)	18.1587(17)	13.205(3)
c / Å	9.755(3)	19.3438(13)	17.133(4)	17.381(4)	17.5671(17)	15.403(4)
α	95.359(3)	90	90	90	90	90
β	103.741(3)	99.313(1)	99.585(3)	97.507(5)	97.715(3)	90
γ	101.365(3)	90	90	90	90	90
V / Å^3	605.5(3)	2457.6(3)	2353.0(10)	4845.0(18)	5026.8(8)	2742.2(11)
Z	1	4	4	4	8	4
ρcalc / g cm^{-3}	1.568	1.530	1.488	1.501	1.447	1.603
μ / mm^{-1}	0.681	0.664	0.687	0.671	0.647	0.626
λ / Å	Mo Kα (0.71073)	Mo Kα (0.71073)	Mo Kα (0.71073)	Mo Kα (0.71073)	Mo Kα (0.71073)	Mo Kα (0.71073)
T / K	100(2)	100(2)	100(2)	100(2)	298(2)	298(2)
$2\theta_{max}$	54.5°	51.5°	52.9°	43.0°	66.3°	51.3°
reflections collected	10828	20406	14164	25167	73381	9924
independent reflections	2719	4702	4807	2444	5967	1311
parameters	224	550	325	378	381	136
R(int)	0.0425	0.0301	0.0458	0.0970	0.1675	0.0377
R1 [I > 2σ(I)]	0.0342	0.0173	0.0688	0.0542	0.0869	0.0953
wR2 (all data)	0.0796	0.0321	0.1891	0.1275	0.2026	0.1852
Largest peak and hole / e Å^{-3}	0.358, -0.276	0.269, -0.205	1.694, -1.690	0.358, -0.303	0.289, -0.302	0.766, -0.501

	$[((3\text{-}NO_2)_2Tp)_2Fe]\cdot CH_2Cl_2$	$[(3\text{-}NH_2Tp)_2Fe]$	$[(3\text{-}NH_2Tp)_2Fe]$	$[((3\text{-}NH_2)_2Tp)_2Fe]$	$[((3\text{-}NH_2)_2Tp)_2Fe]$
CCDC number	2017281	2018042	2018043	2017278	2017279
Formula	$C_{18}H_{16}B_2FeN_{16}O_8$, $(CH_2Cl_2)_{0.91}$	$C_{18}H_{22}B_2FeN_{14}$	$C_{18}H_{22}B_2FeN_{14}$	$C_{18}H_{24}B_2FeN_{16}$	$C_{18}H_{24}B_2FeN_{16}$
Fw / g mol^{-1}	739.22	511.48	511.96	542.00	542.00
Crystal size / mm^3	0.43, 0.28, 0.36	0.062, 0.21, 0.32	0.062, 0.21, 0.32	0.21, 0.51, 0.25	0.21, 0.51, 0.25
crystal system	monoclinic	triclinic	triclinic	trigonal	trigonal
space group	$P2_1/c$	P-1	P-1	*R-3*	*R-3*
a / Å	15.7878(7)	9.2821(12)	9.439(3)	9.093(2)	9.174(2)
b / Å	9.5340(5)	10.1947(13)	10.374(3)	9.093(2)	9.174(2)
c / Å	19.5945(10)	13.4103(17)	13.566(4)	25.043(2)	26.393(2)
α	90	85.767(3)	85.264(4)	90	90
β	99.2920(10)	80.397(3)	80.233(4)	90	90
γ	90	63.053(3)	63.663(4)	120	120
V / $Å^3$	2910.7(2)	1115.4(2)	1173.2(6)	1793.3(2)	1923.8(2)
Z	4	2	2	3	3
ρcalc / g cm^{-3}	1.687	1.523	1.449	1.506	1.404
μ / mm^{-1}	0.778	0.717	0.682	0.676	0.630
λ / Å	Mo Kα (0.71073)	Mo Kα (0.71073)	Mo Kα (0.71073)	Mo Kα (0.71073)	Mo Kα (0.71073)
T / K	100(2)	100(2)	298 (2)	100(2)	298 (2)
2θmax	54.3°	52.8°	50.9°	72.7°	61.1°
reflections collected	45979	29668	10705	13794	11006
independent reflections	6423	4572	4347	8416	1306
parameters	498	356	357	62	63
R(int)	0.0497	0.0429	0.0242	0.0372	0.0232
R1 [$I > 2\sigma(I)$]	0.0316	0.0705	0.0587	0.0374	0.0318
wR2 (all data)	0.0788	0.1697	0.1448	0.0991	0.0942
Largest peak and hole / e $Å^{-3}$	0.698, -0.588	0.478, -0.489	0.332, -0.260	0.926, -0.891	0.257, -0.232

Solid-state packing in all compounds

Packing of TBA[3-NO_2Tp] in the crystal lattice.

a.)

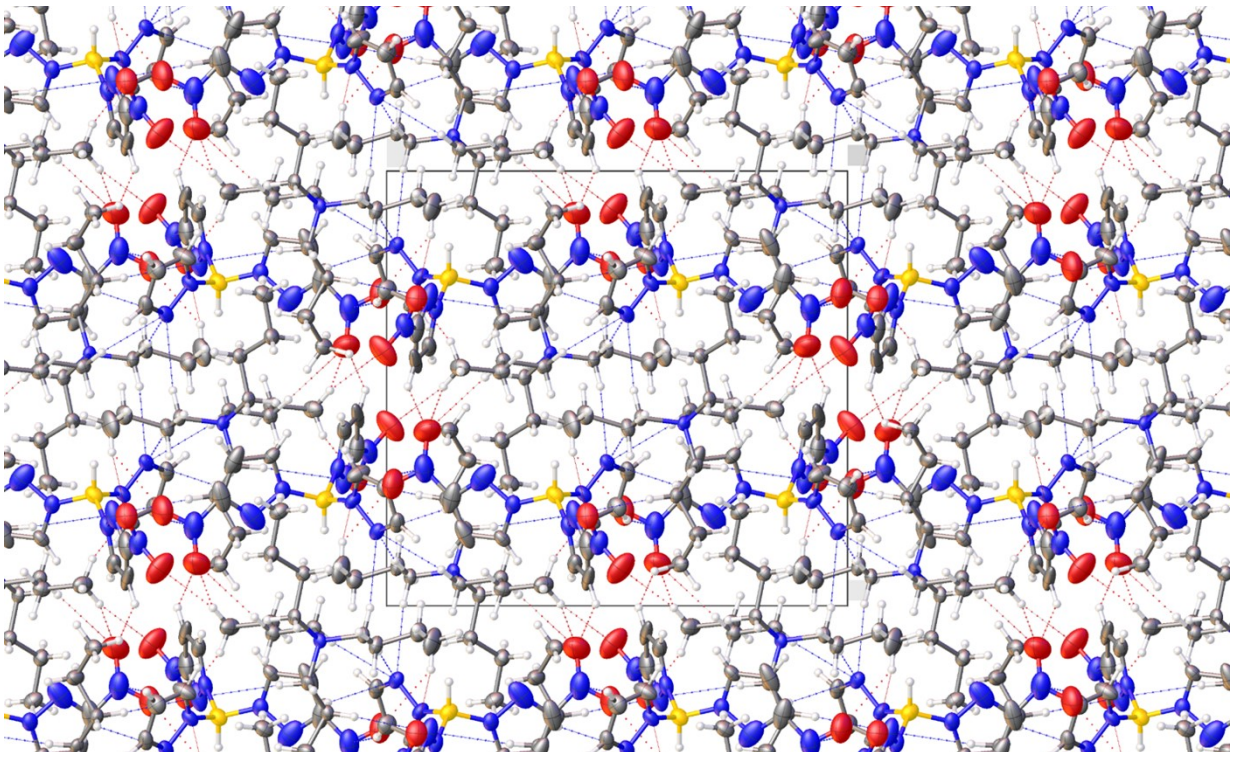

b.)

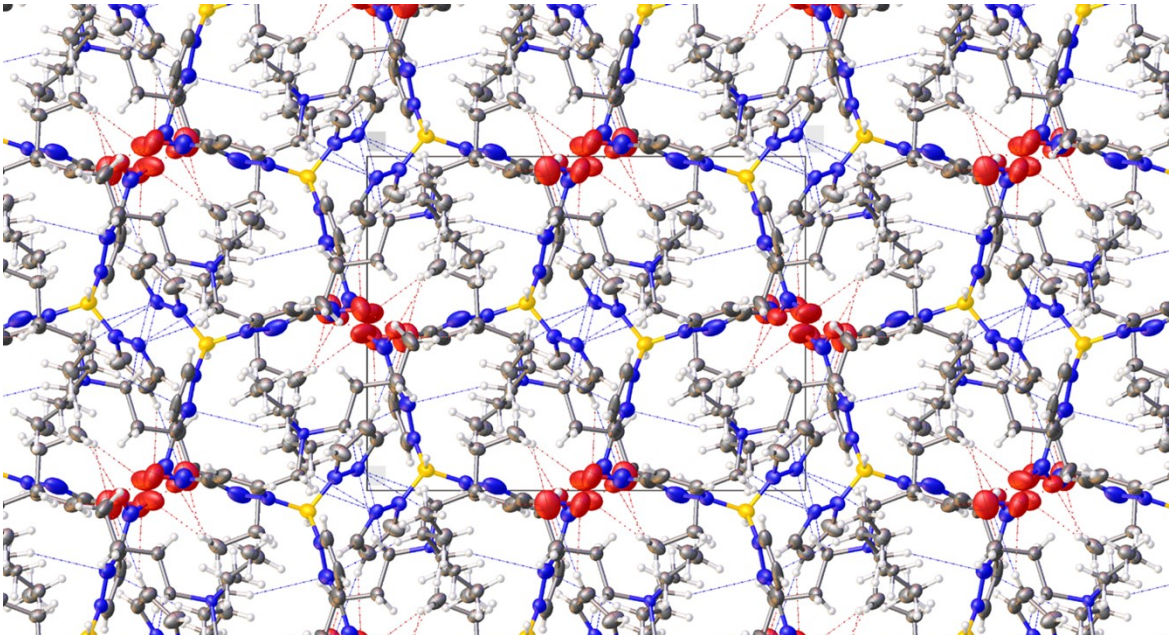

Figure 11. Non-classical hydrogen bonds are observed between 1.) oxygen positions of disordered nitro group and TBA^+ hydrogen site with donor···acceptor distances of 2.236-2.831 Å. 2.) nitrogen position of pyrazole and TBA^+ hydrogen site with donor···acceptor distances of 2.717-2.851 Å. 3.) oxygen positions of disordered nitro group and pyrazole hydrogen site with donor···acceptor distances of 2.540 Å. 4.) nitrogen position of disordered nitro group and pyrazole hydrogen site with donor···acceptor distances of 2.815 Å. a). Projection along [100]. b). Projection along [001].

Packing of TBA[4-NO_2Tp] in the crystal lattice.

a.)

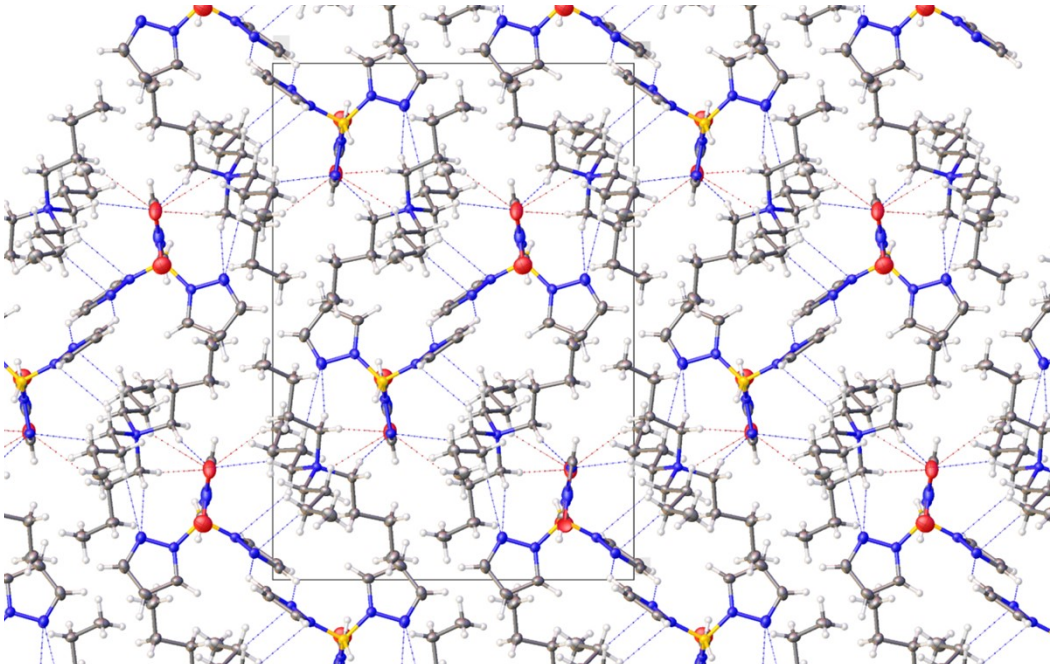

b.)

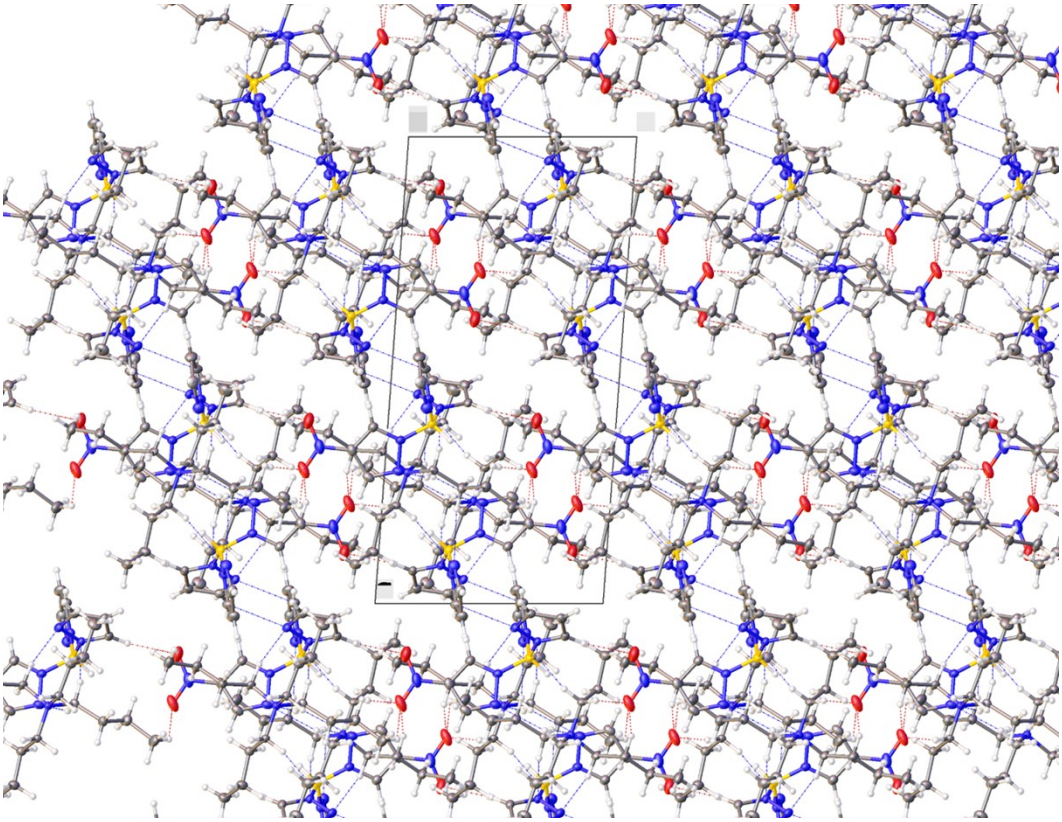

Figure 12. Non-classical hydrogen bonds are observed between 1.) oxygen positions of nitro group and TBA^+ hydrogen site with donor…acceptor distances of 2.494-2.750 Å.2.) nitrogen position of pyrazole and TBA^+ hydrogen site with donor…acceptor distances of 2.673-2.757 Å. 3.) oxygen positions of nitro group and pyrazole hydrogen site with donor…acceptor distances of 2.680 Å. a). Projection along [100]. b). Projection along [010].

Packing of $[(3\text{-}NO_2Tp)_2Fe]$ in the crystal lattice.

a.)

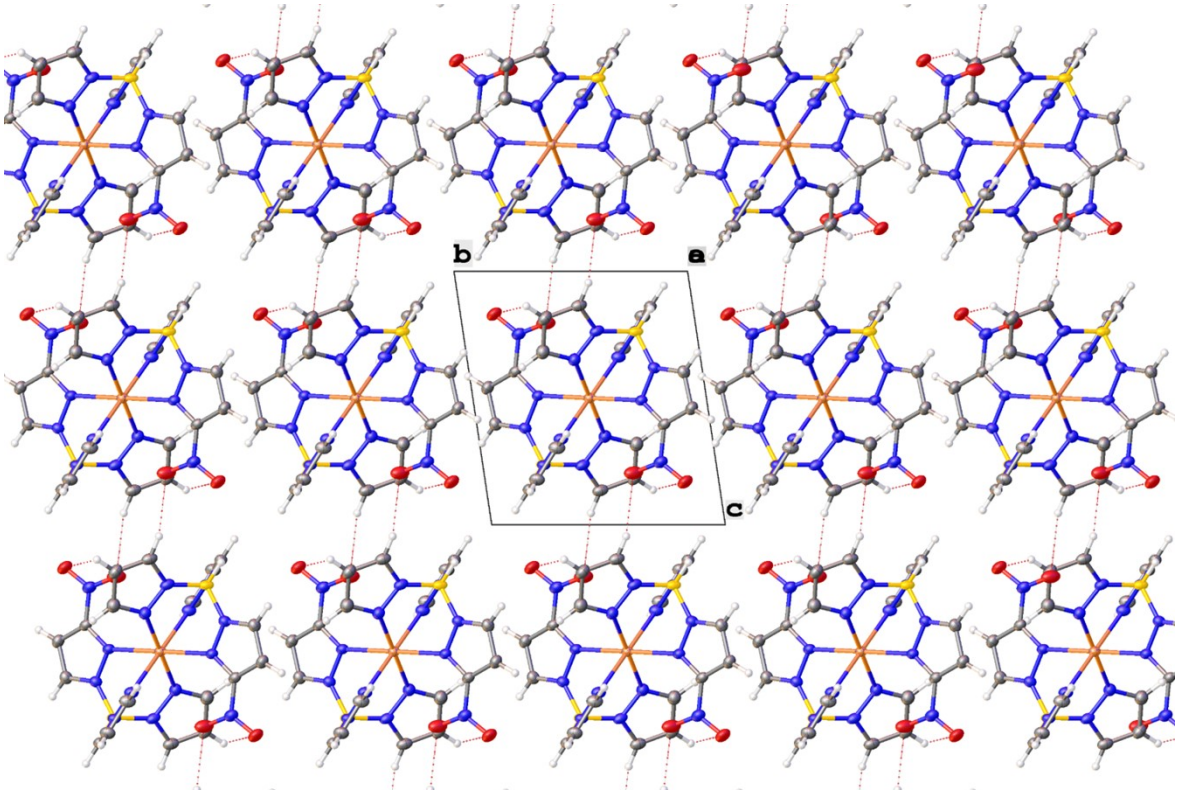

a.)

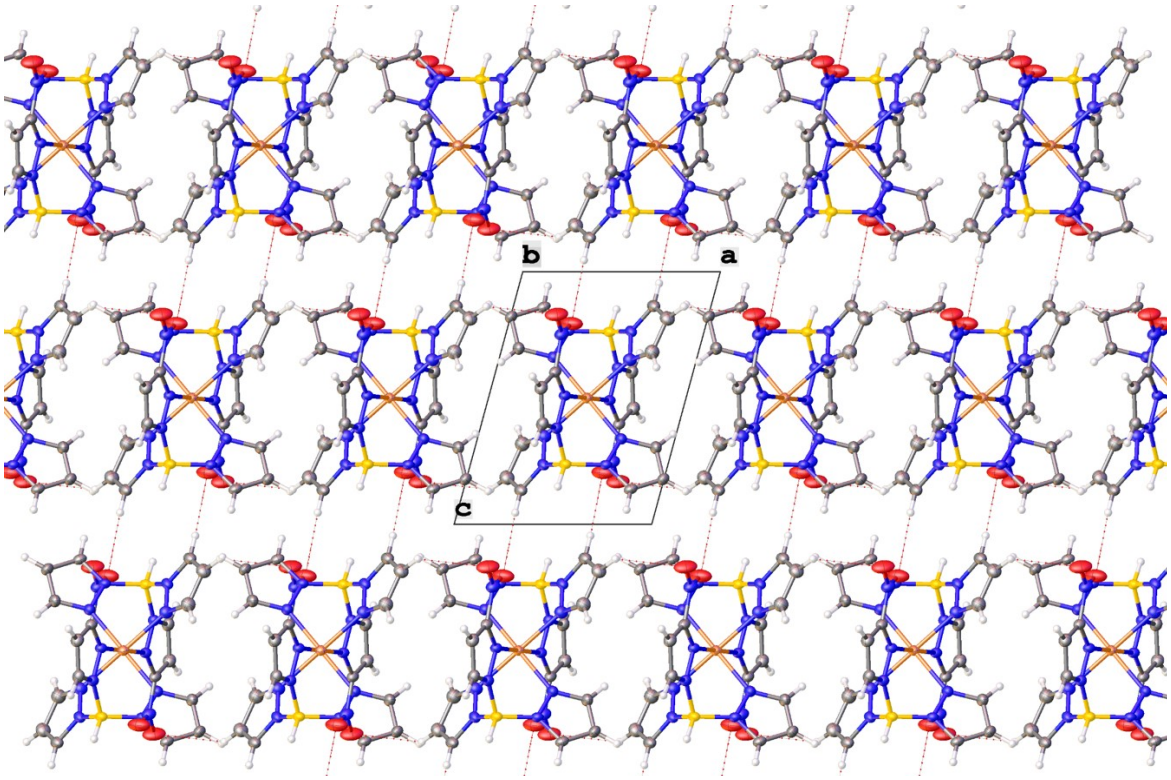

Figure 13. Non-classical hydrogen bonds are observed between oxygen positions of nitro group and pyrazole hydrogen site with donor···acceptor distances of 2.422-2.709 Å. a). Projection along [100]. b). Projection along [010].

Packing of [(Tp)Fe(3-NO_2Tp)]· $(C_6H_6)_{0.5}$ in the crystal lattice.

a.)

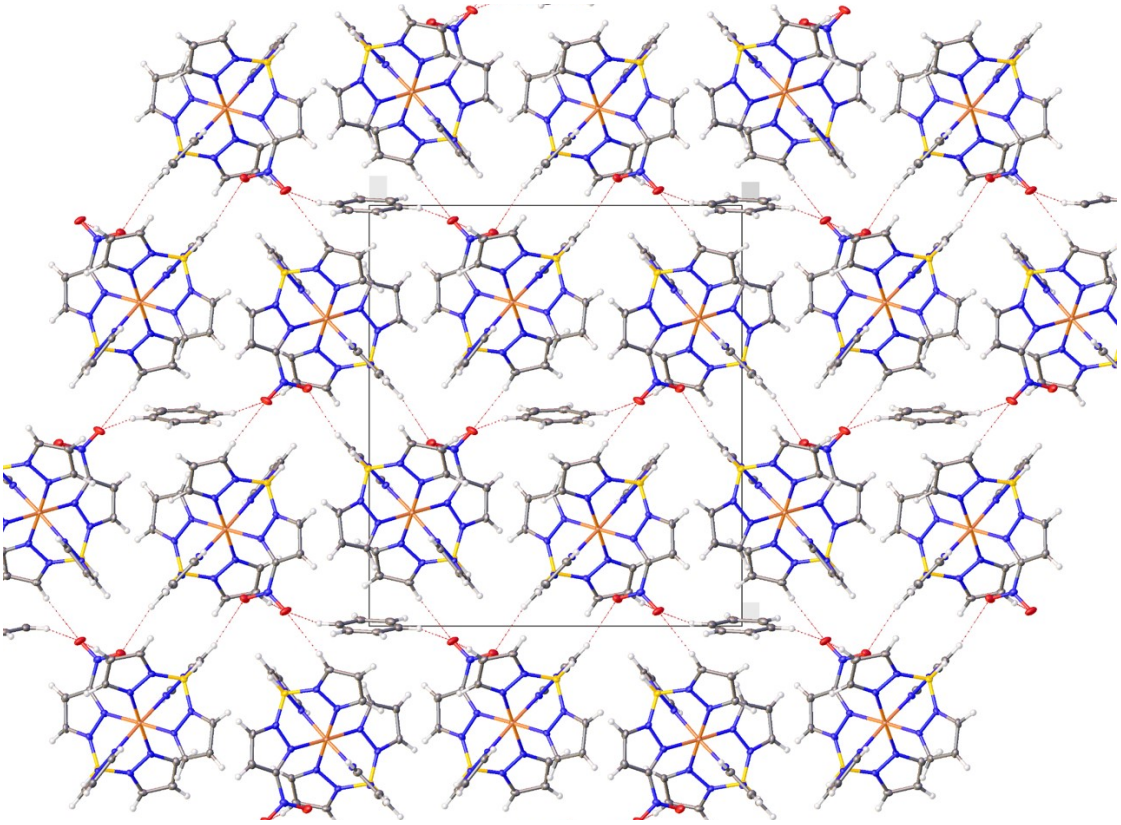

b.)

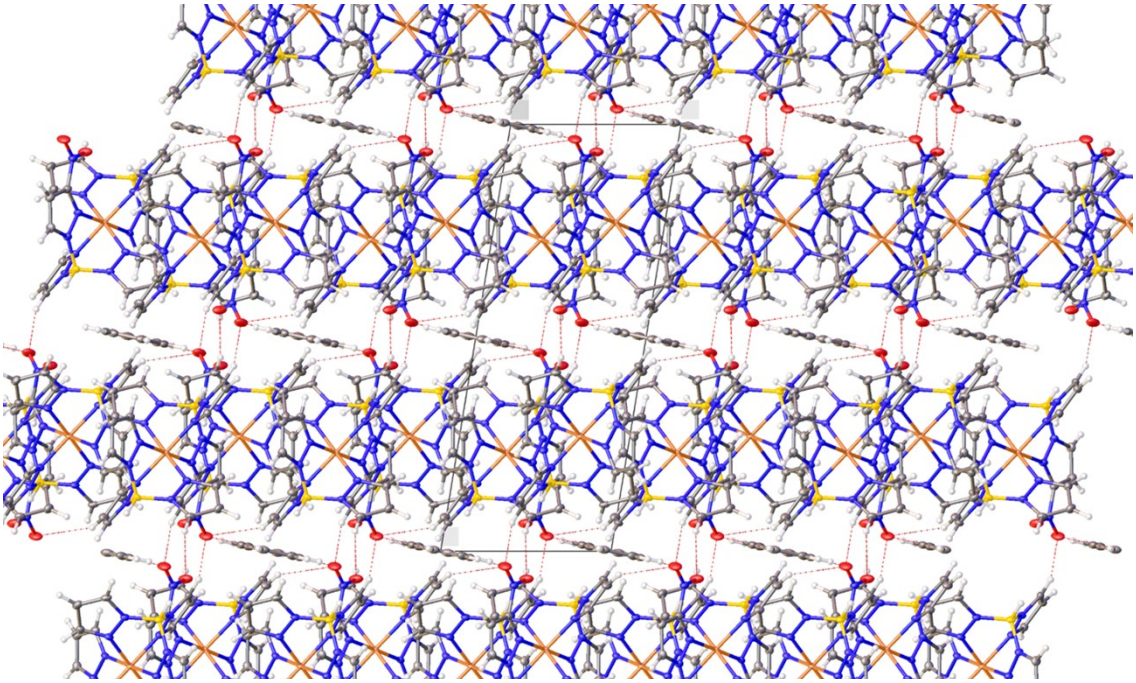

Figure 14. Non-classical hydrogen bonds are observed between 1.) oxygen positions of nitro group and benzene hydrogen site with donor···acceptor distances of 2.839 Å. 2.) oxygen positions of nitro group and pyrazole hydrogen site with donor···acceptor distances of 2.501-2.663 Å. a). Projection along [100]. b). Projection along [010].

Packing of [(Tp)Fe(4-NO_2Tp)] in the crystal lattice.

a.)

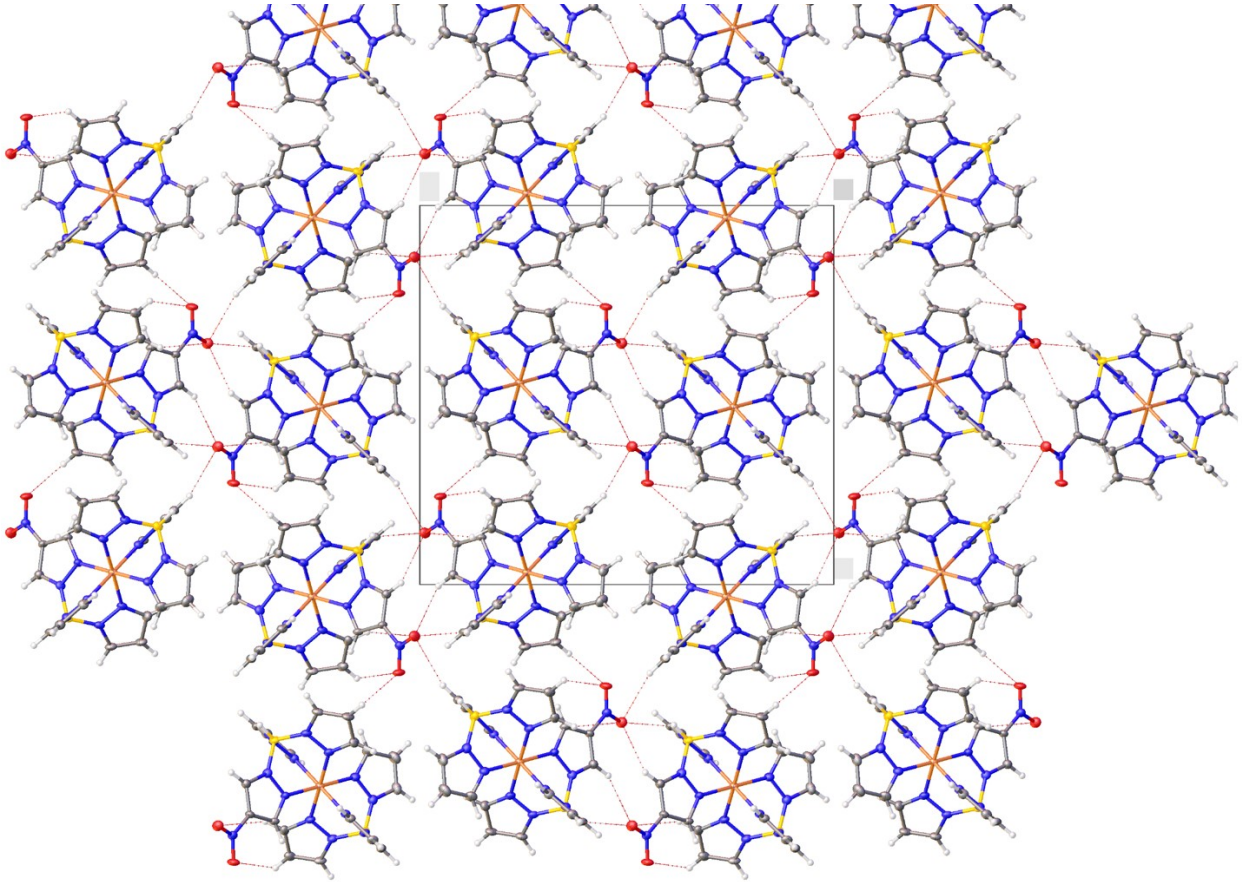

b.)

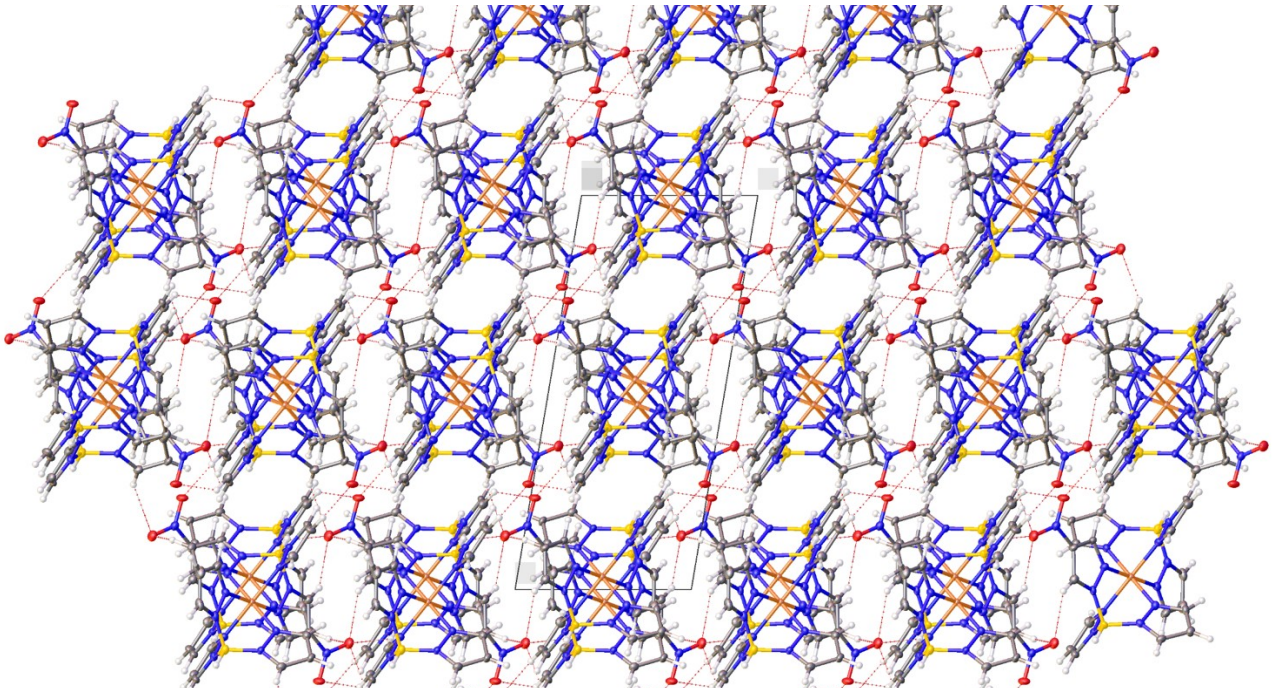

Figure 15. Non-classical hydrogen bonds are observed between oxygen positions of nitro group and pyrazole hydrogen site with donor···acceptor distances of 2.482-2.663 Å. a). Projection along [100]. b). Projection along [010].

Packing of [(Tp)Fe(5-NO_2Tp)]· $(CH_3CN)_{0.5}$ in the crystal lattice.

a.)

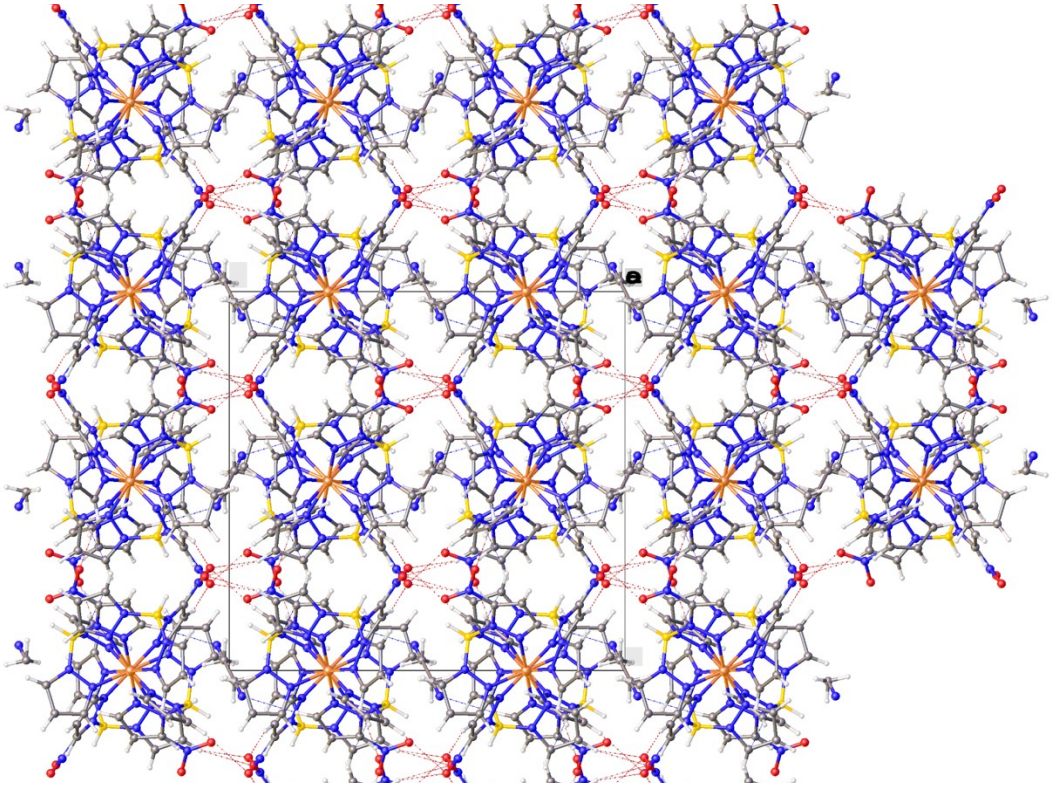

b.)

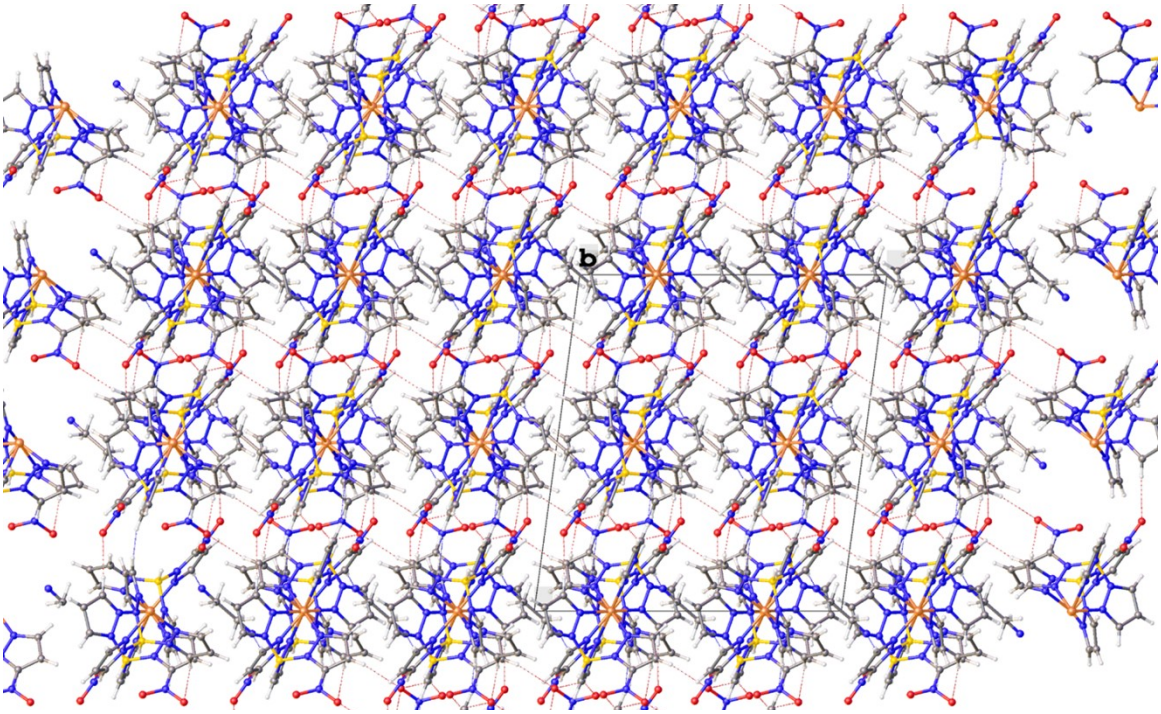

Figure 16. Non-classical hydrogen bonds are observed between 1). oxygen positions of nitro group and pyrazole hydrogen site with donor···acceptor distances of 2.426-2.752 Å. 2). nitrogen position of disordered acetonitrile and pyrazole hydrogen site with donor···acceptor distances of 2.690 Å. 3). nitrogen position of pyrazole and pyrazole hydrogen site with donor···acceptor distances of 2.866 Å. a). Projection along [100]. b). Projection along [010].

Packing of [((3-NO_2)$_2$Tp)$_2$Fe] in the crystal lattice.

a.)

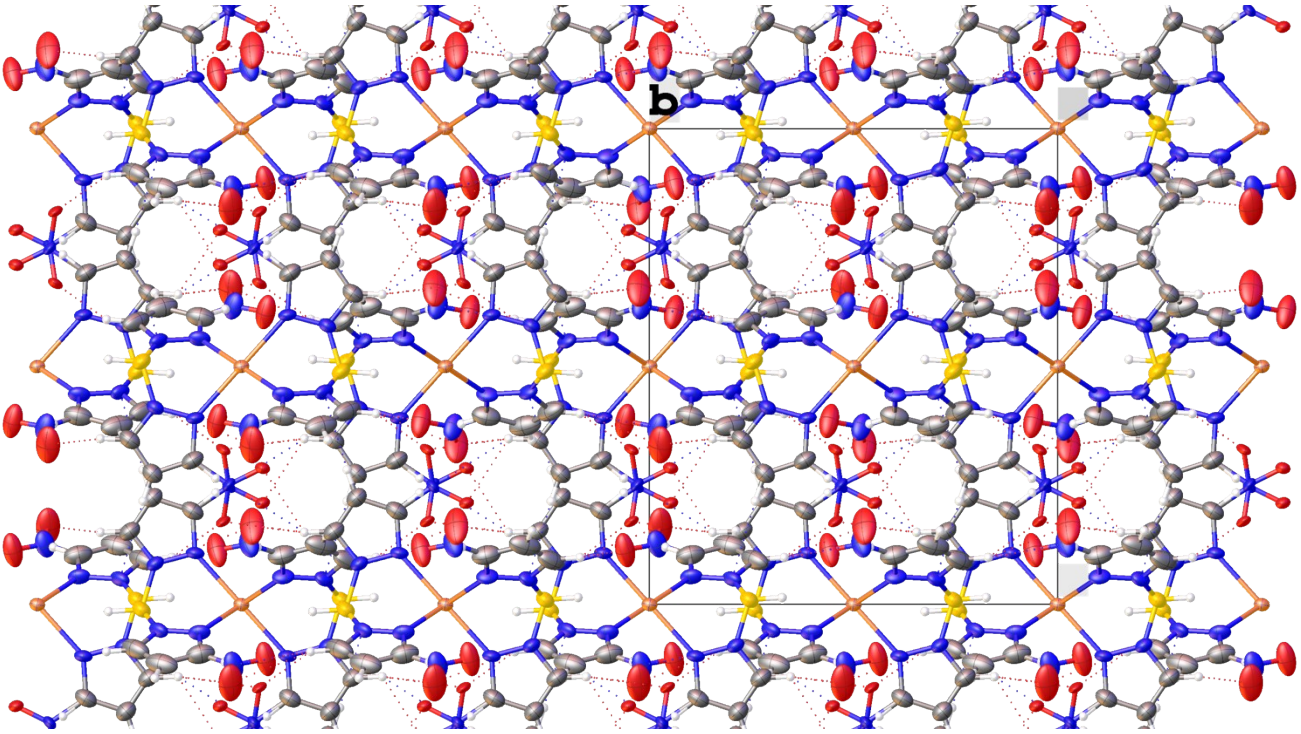

b.)

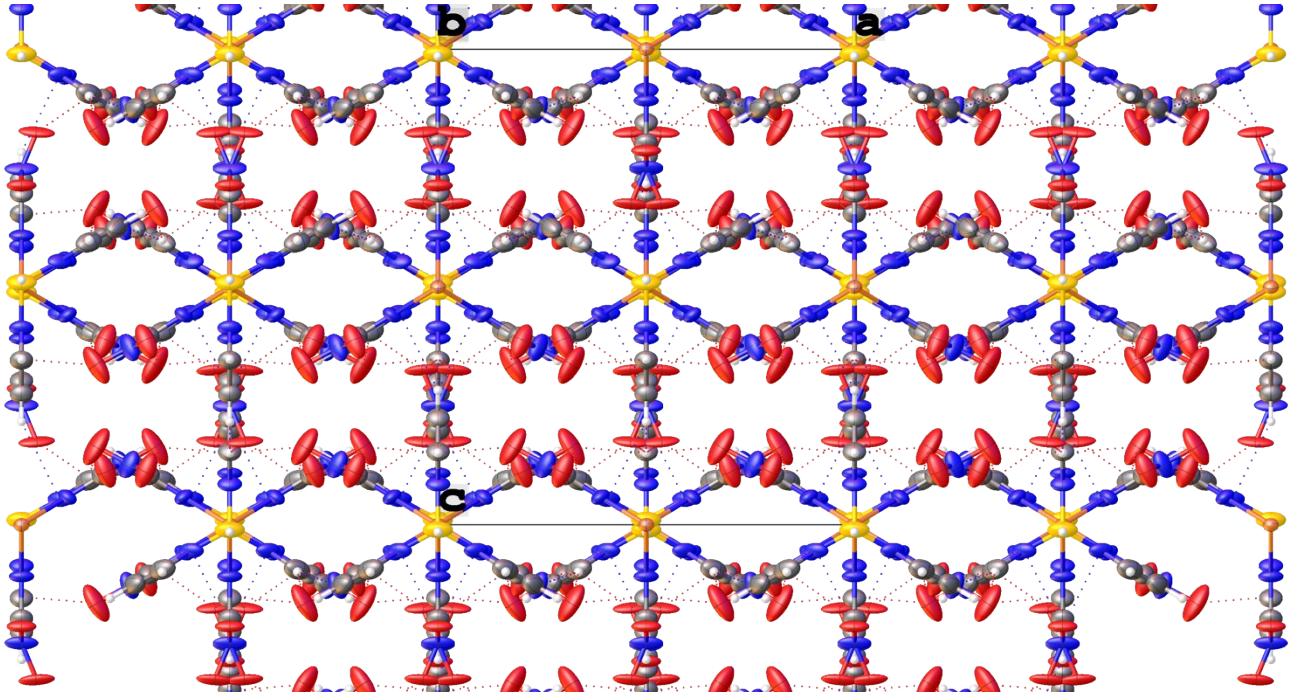

Figure 17. Non-classical hydrogen bonds are observed between 1). oxygen positions of nitro group and pyrazole hydrogen site with donor···acceptor distances of 2.486-2.964 Å. 2). nitrogen position of nitro group and pyrazole hydrogen site with donor···acceptor distances of 2.852-2.893 Å. 3). nitrogen position of pyrazole and pyrazole hydrogen site with donor···acceptor distances of 2.904 Å. a). Projection along [100]. b). Projection along [010].

Packing of $[((3\text{-}NO_2)_2Tp)_2Fe]\cdot CH_2Cl_2$ in the crystal lattice.

a.)

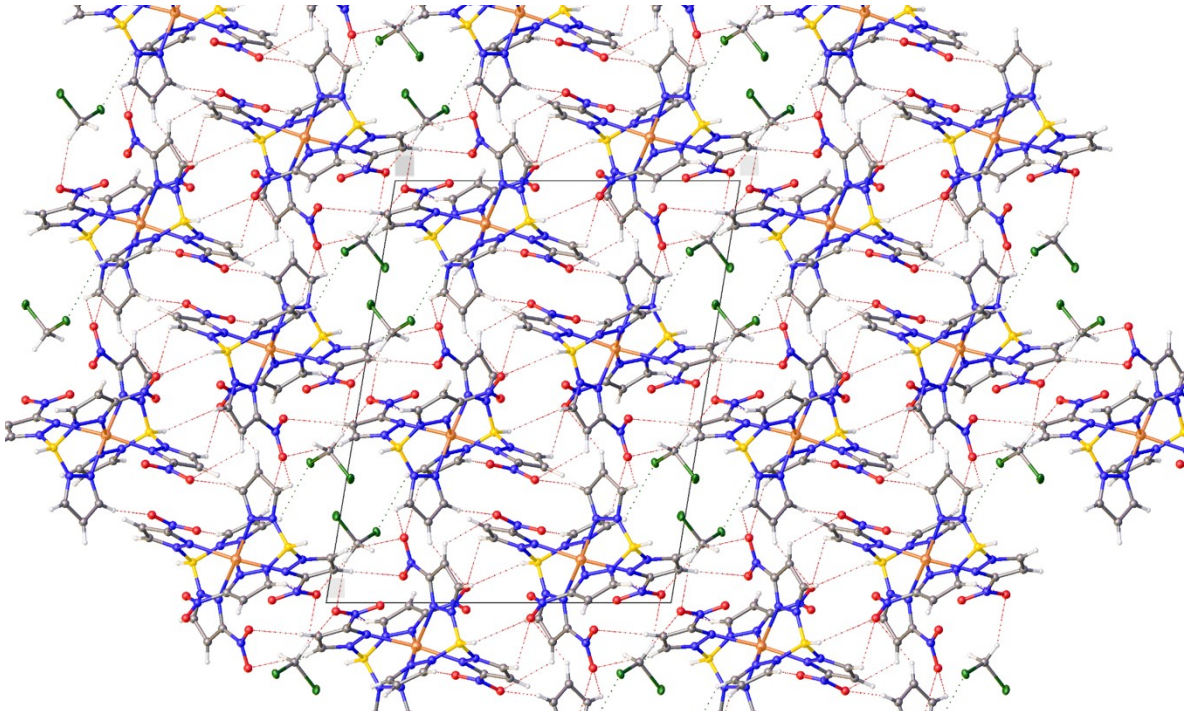

b.)

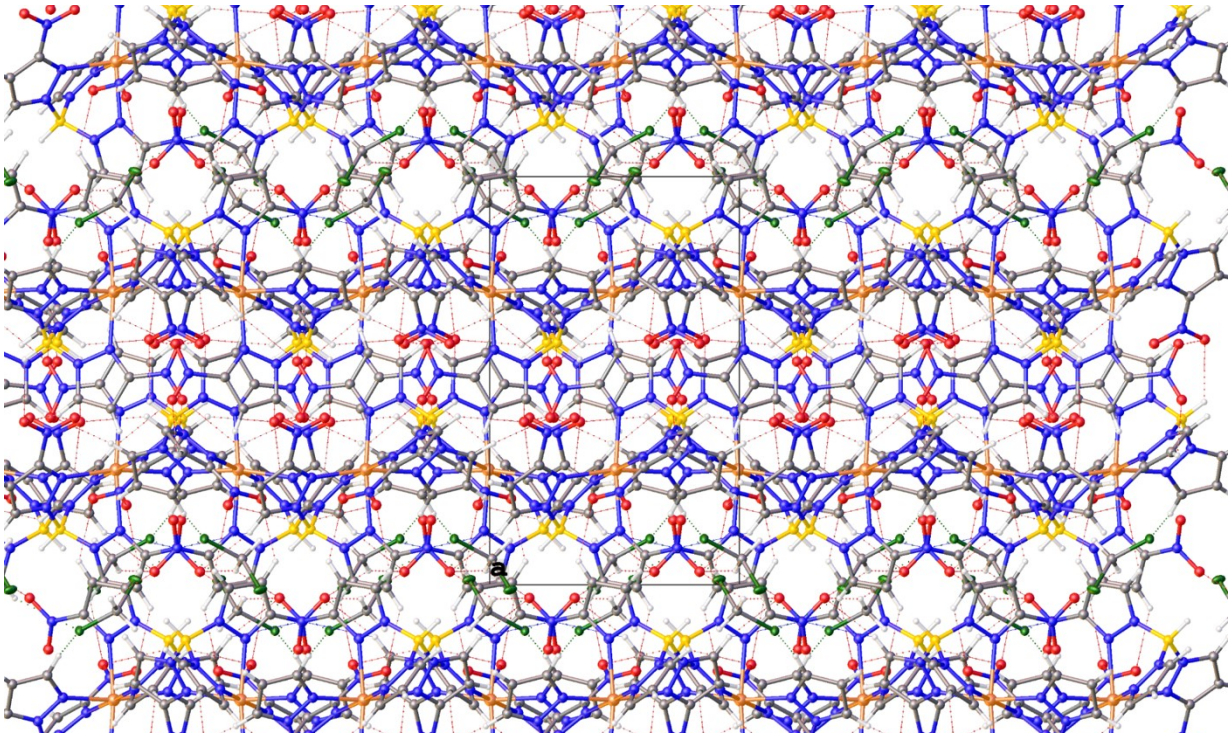

Figure 18. Non-classical hydrogen bonds are observed between 1.) chloride positions of dichloromethane and pyrazole hydrogen site with donor…acceptor distances of 3.046 Å. 2.) oxygen positions of nitro group and pyrazole hydrogen site with donor…acceptor distances of 2.392-2.723 Å. 3.) oxygen positions of nitro group and boron hydrogen site with donor…acceptor distances of 2.829 Å. 4.) oxygen positions of nitro group and dichloromethane hydrogen site with donor…acceptor distances of 2.639-2.733 Å. a). Projection along [010]. b). Projection along [001].

Packing of [(3-NH_2Tp)$_2$Fe] in the crystal lattice.

a.)

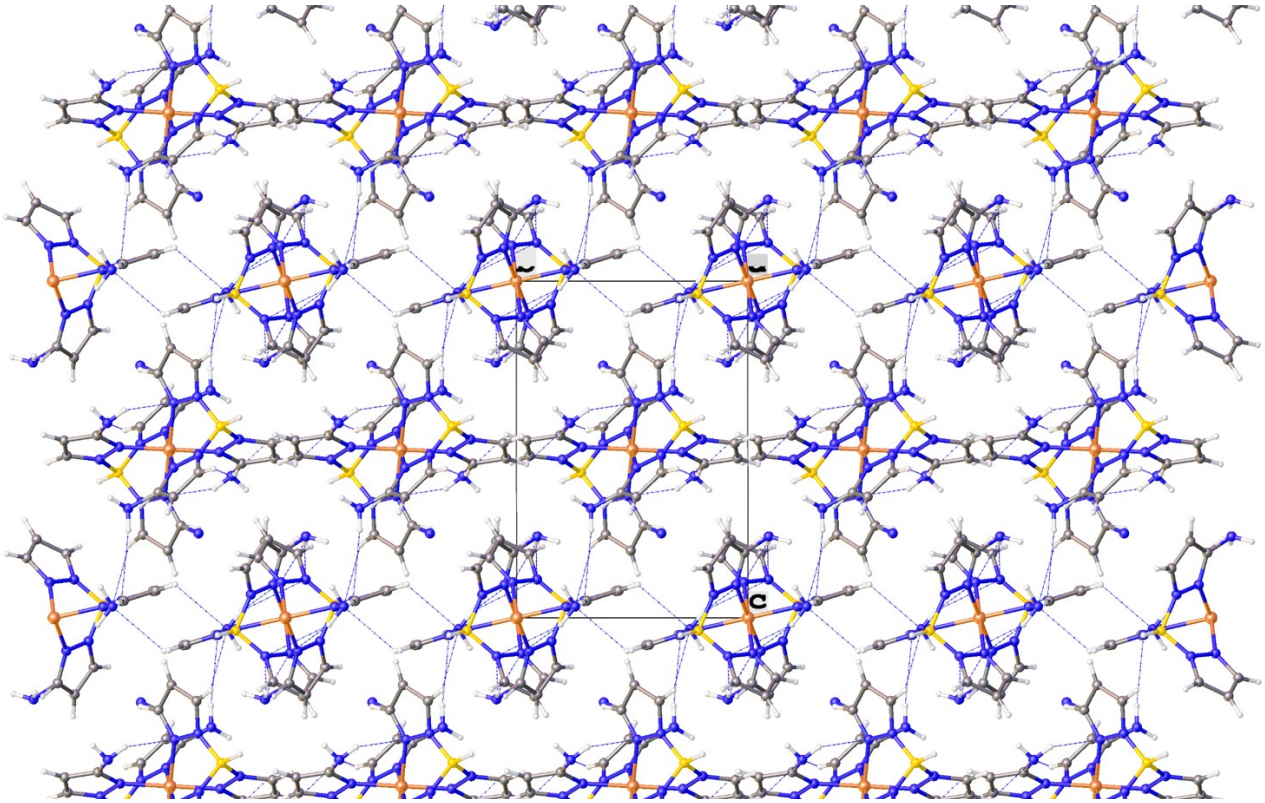

b.)

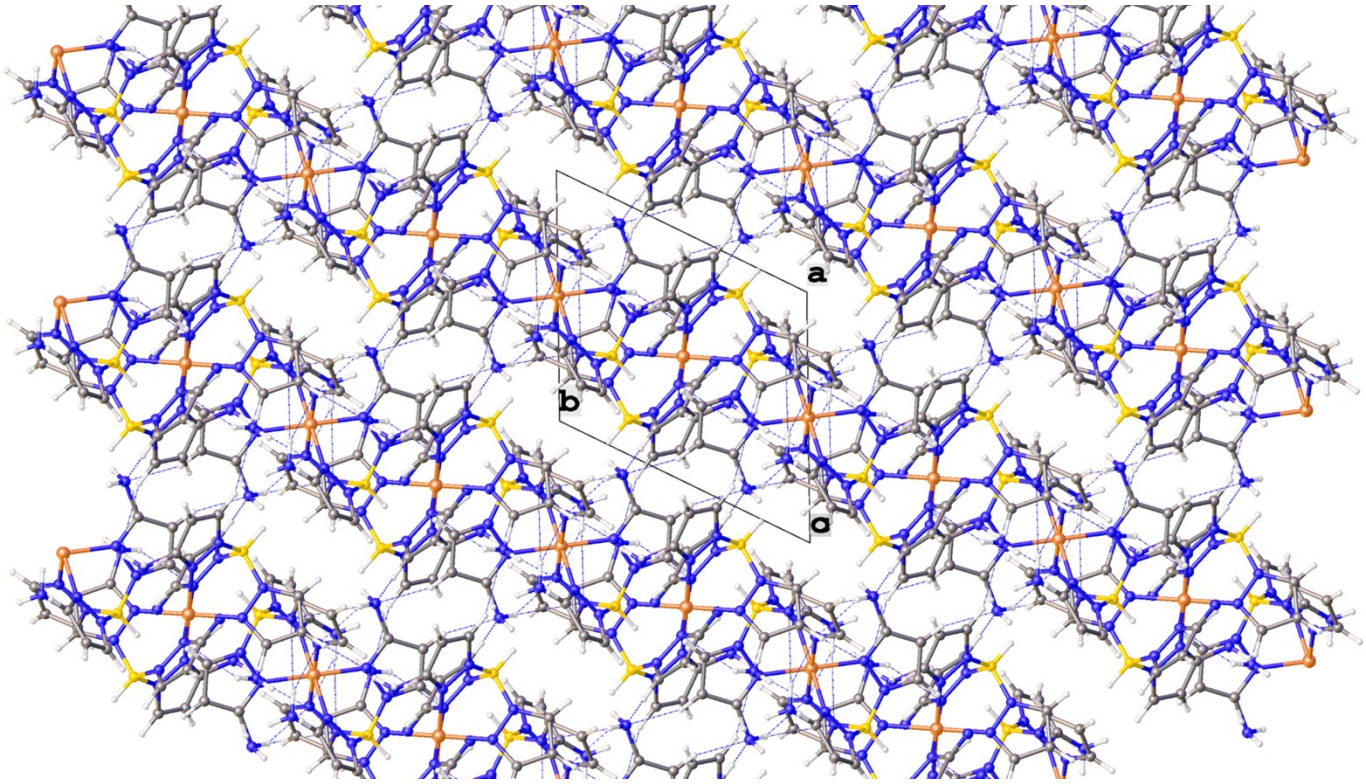

Figure 19. Non-classical hydrogen bonds are observed between 1). nitrogen positions of disordered amino group and pyrazole hydrogen site with donor⋯acceptor distances of 2.562-2.822 Å. 2). nitrogen position of pyrazole and amino hydrogen site with donor⋯acceptor distances of 2.250-2.879 Å. a). Projection along [100]. b). Projection along [001].

Packing of [((3-NH_2)$_2$Tp)$_2$Fe] in the crystal lattice.

a.)

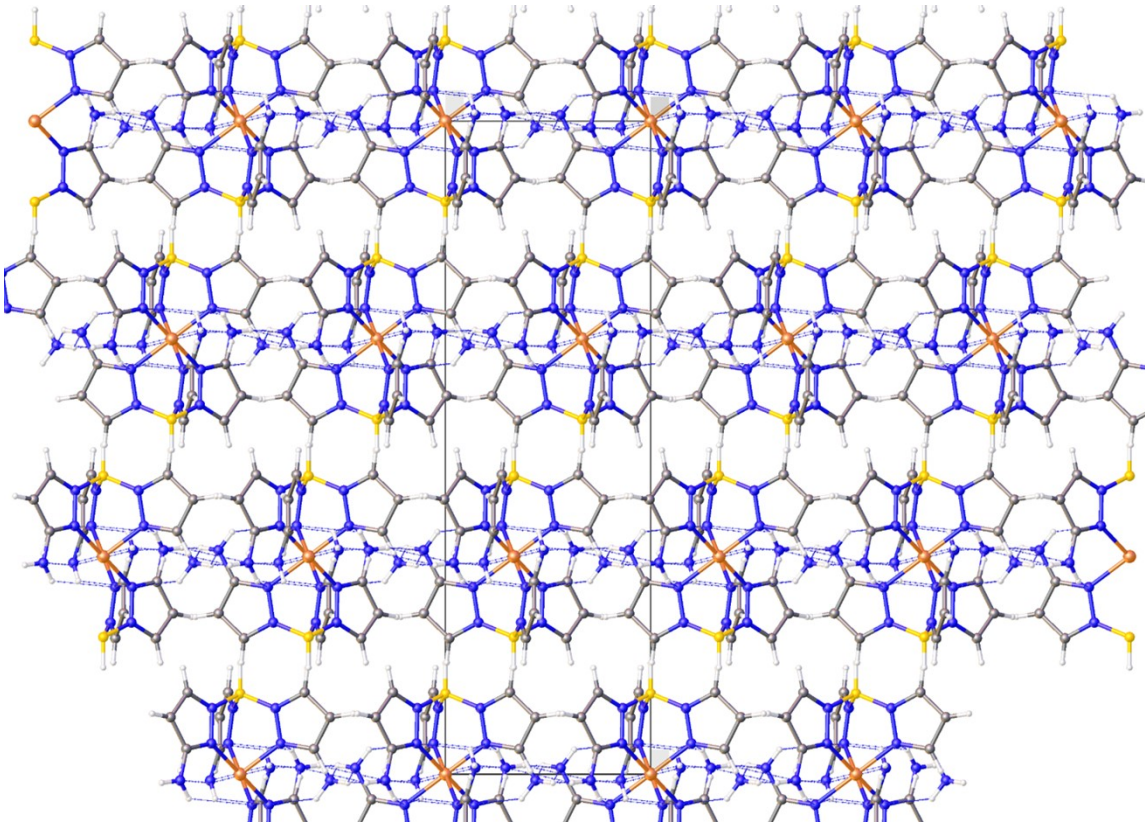

b.)

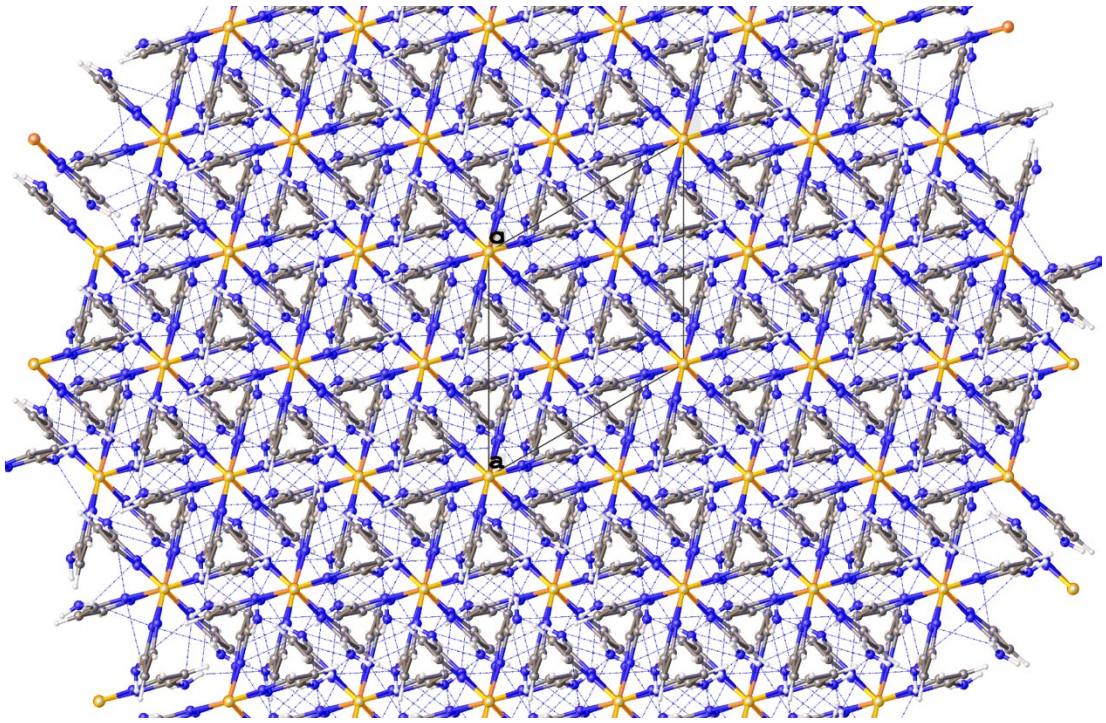

Figure 20. Non-classical hydrogen bonds are observed between 1). nitrogen positions of disordered amino group and disordered amino hydrogen site with donor…acceptor distances of 2.607-2.859 Å. 2). nitrogen

position of pyrazole and amino hydrogen site with donor…acceptor distances of 2.540-2.661 Å. a). Projection along [100]. b). Projection along [001].

PXRD spectra:

[(3-NO_2Tp)$_2$Fe]

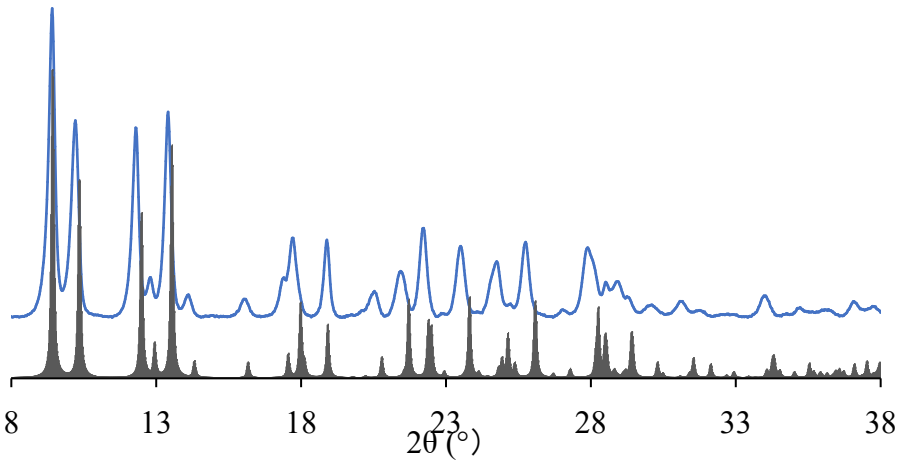

Figure 21. Powder X-ray diffraction patterns for [(3-NO_2Tp)$_2$Fe] crystals. The room temperature experimental PXRD pattern is represented as blue curve. The diffraction pattern calculated from the single crystal structure at 100 K is represented in black.

[(Tp)Fe(3-NO_2Tp)]· (C_6H_6)$_{0.5}$

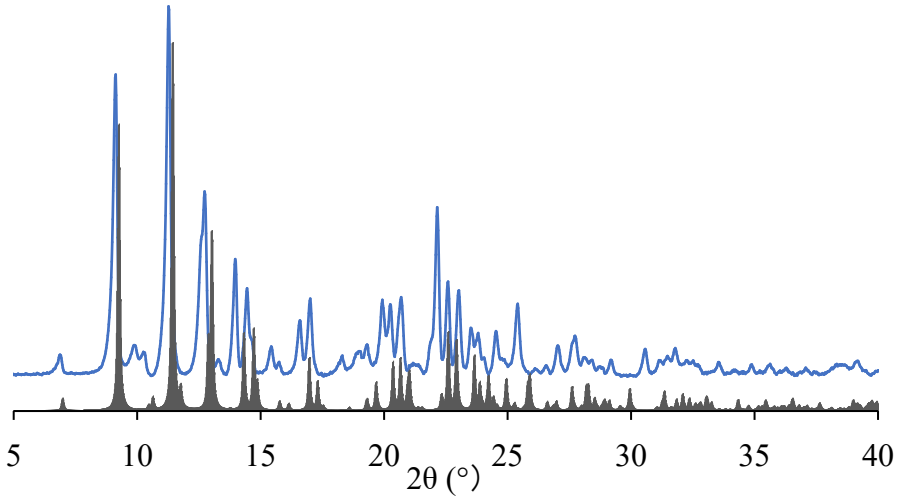

Figure 22. Powder X-ray diffraction patterns for [(Tp)Fe(3-NO_2Tp)]· (C_6H_6)$_{0.5}$ crystals. The room temperature experimental PXRD pattern is represented as blue curve. The diffraction pattern calculated from the single crystal structure at 100 K is represented in black.

[(Tp)Fe(4-NO_2Tp)]

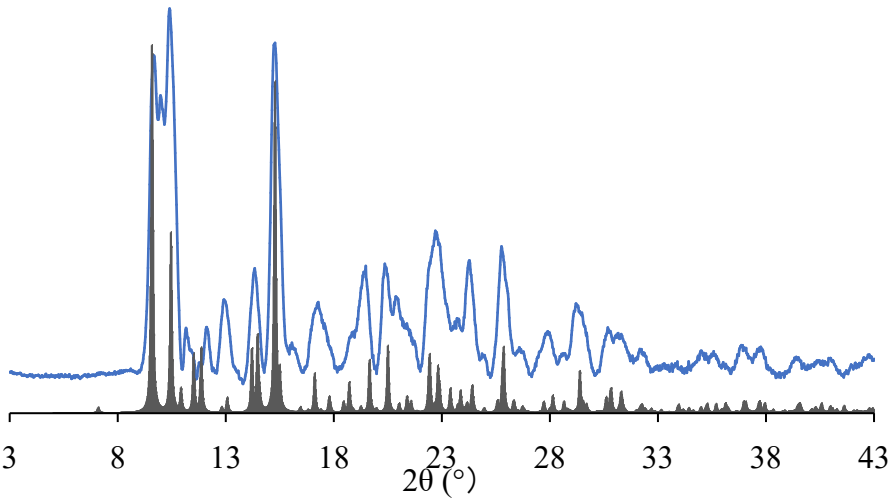

Figure 23. Powder X-ray diffraction patterns for [(Tp)Fe(4-NO_2Tp)] crystals. The room temperature experimental PXRD pattern is represented as blue curve. The diffraction pattern calculated from the single crystal structure at 100 K is represented in black.

[(Tp)Fe(5-NO_2Tp)]

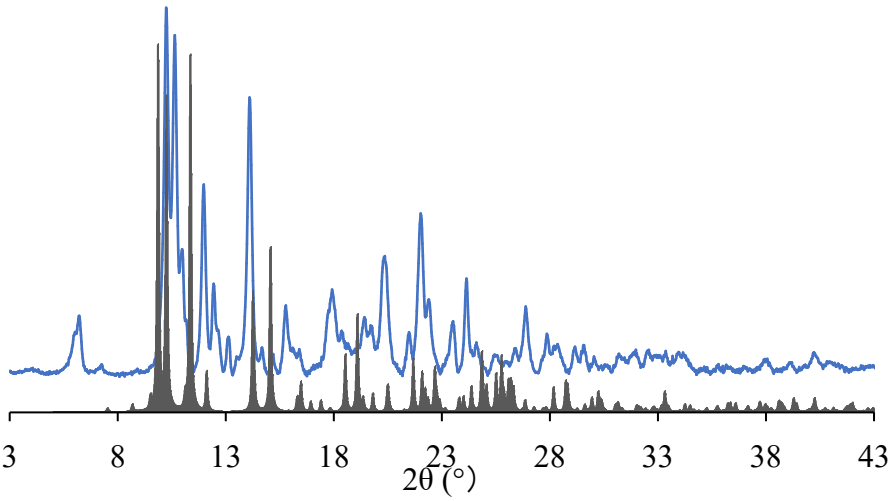

Figure 24. Powder X-ray diffraction patterns for desolvated [(Tp)Fe(5-NO_2Tp)] crystals. It differs from the diffraction pattern calculated from the single crystal structure at 100 K of [(Tp)Fe(5-NO_2Tp)]·$(CH_3CN)_{0.5}$ (in black).

[$((3\text{-}NO_2)_2Tp)_2Fe$]

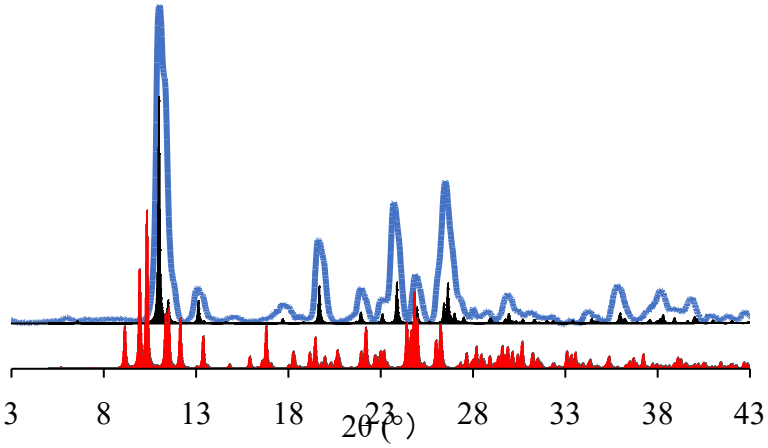

Figure 25. Powder X-ray diffraction pattern for de-solvated [$((3\text{-}NO_2)_2Tp)_2Fe]\cdot CH_2Cl_2$ crystals (blue). It differs from the diffraction pattern calculated from the single crystal structure at 100 K of [$((3\text{-}NO_2)_2Tp)_2Fe]\cdot CH_2Cl_2$ (in red), but fits the diffraction pattern for [$((3\text{-}NO_2)_2Tp)_2Fe$] calculated from the crystal structure at 298 K is in black.

[$(3\text{-}NH_2Tp)_2Fe$]

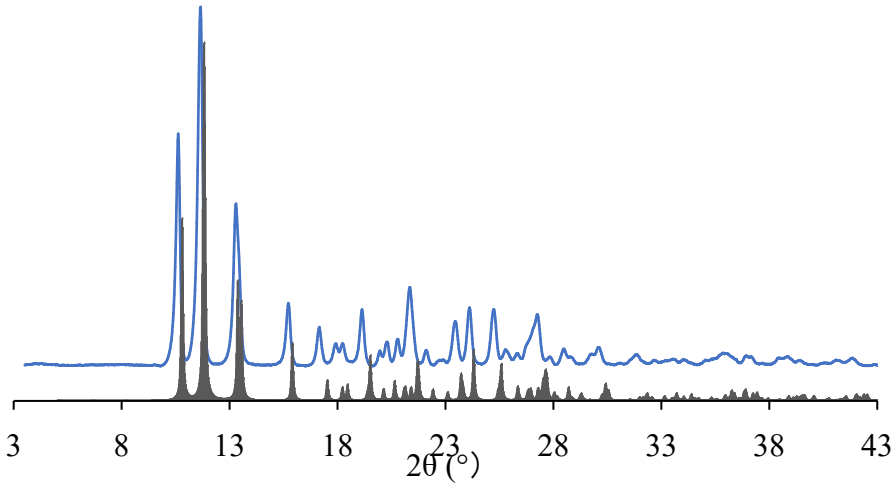

Figure 26. Powder X-ray diffraction patterns for [$(3\text{-}NH_2Tp)_2Fe$] crystals. The room temperature experimental PXRD pattern is represented as blue curve. The diffraction pattern calculated from the single crystal structure at 100 K is represented in black.

[((3-NH_2)$_2$Tp)$_2$Fe]

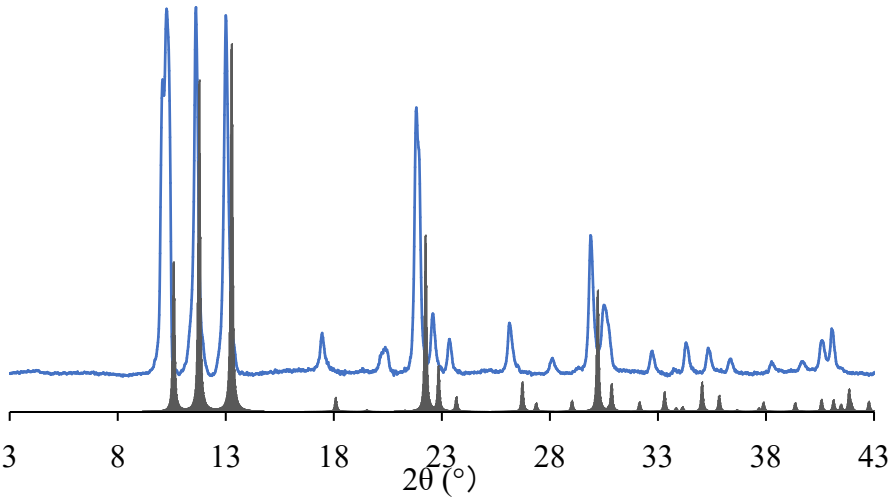

Figure 27. X-ray diffraction patterns for [((3-NH_2)$_2$Tp)$_2$Fe] crystals. The room temperature experimental PXRD pattern is represented as blue curve. The diffraction pattern calculated from the single crystal structure at 100 K is represented in black.

IR spectra:

TBA[4-NO_2Tp]

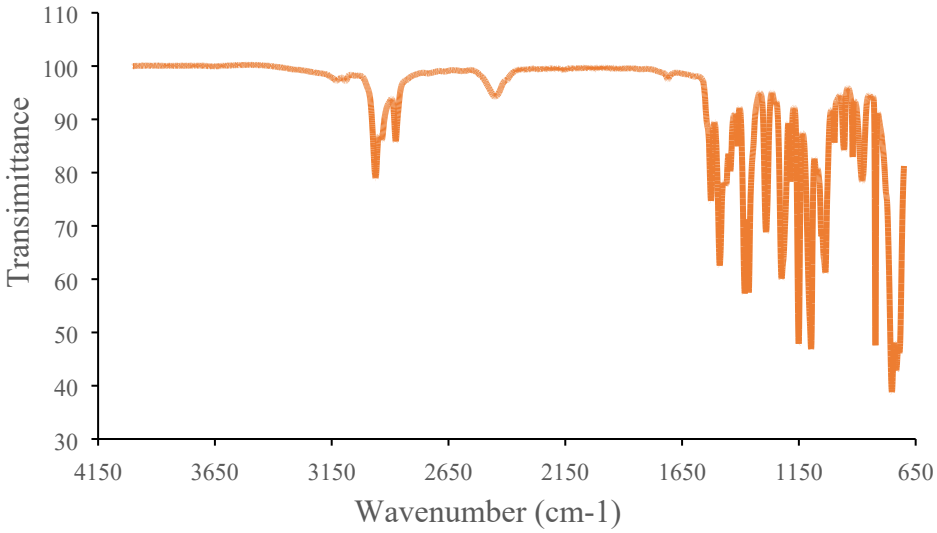

TBA[3-NO_2Tp]

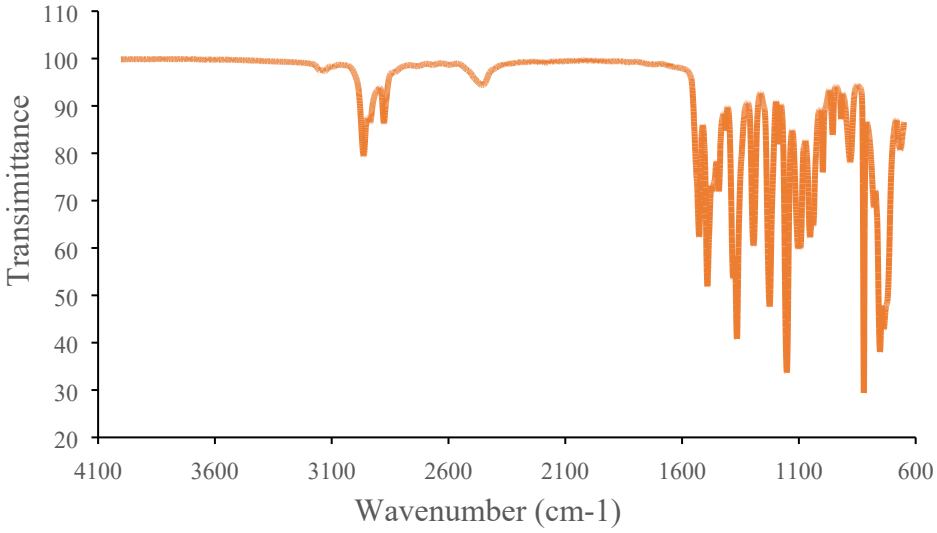

[(3-NO_2Tp)$_2$Fe]

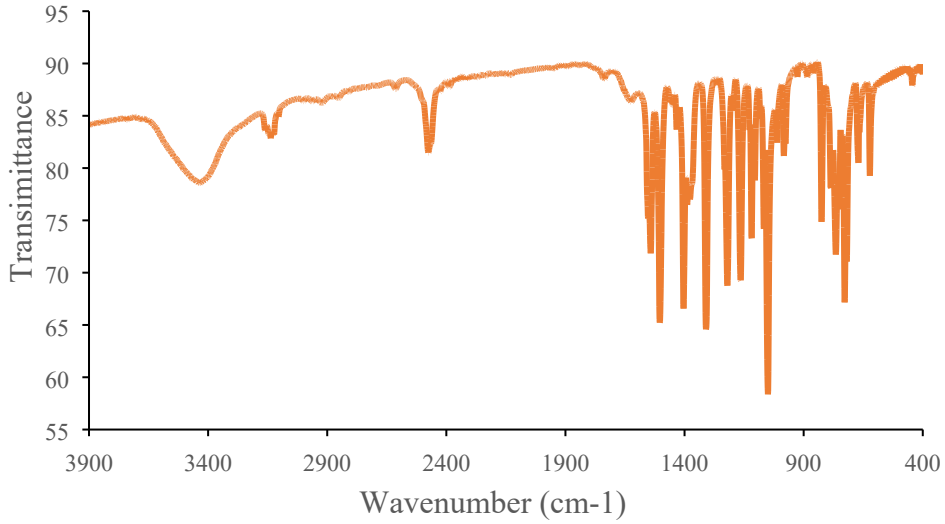

[(Tp)Fe(3-NO_2Tp)]·(C_6H_6)$_{0.5}$

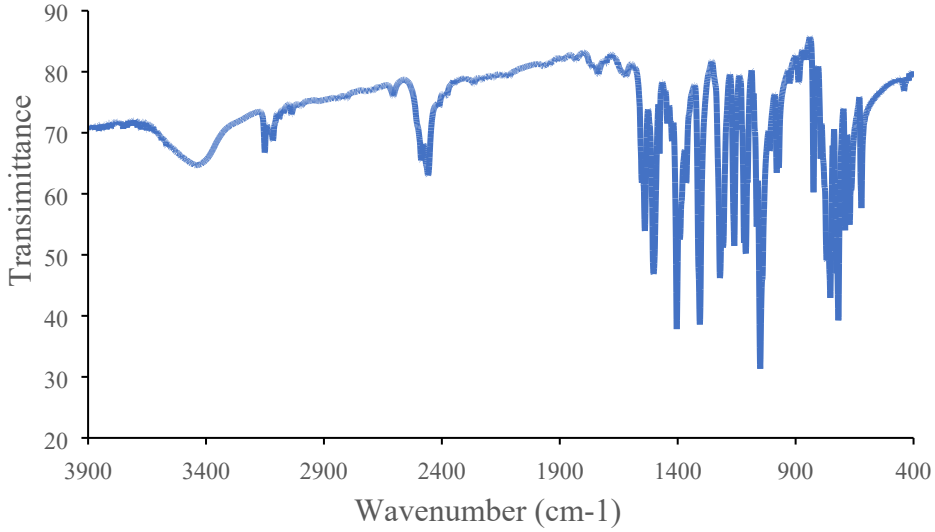

[((3-NO_2)$_2$Tp)$_2$Fe]

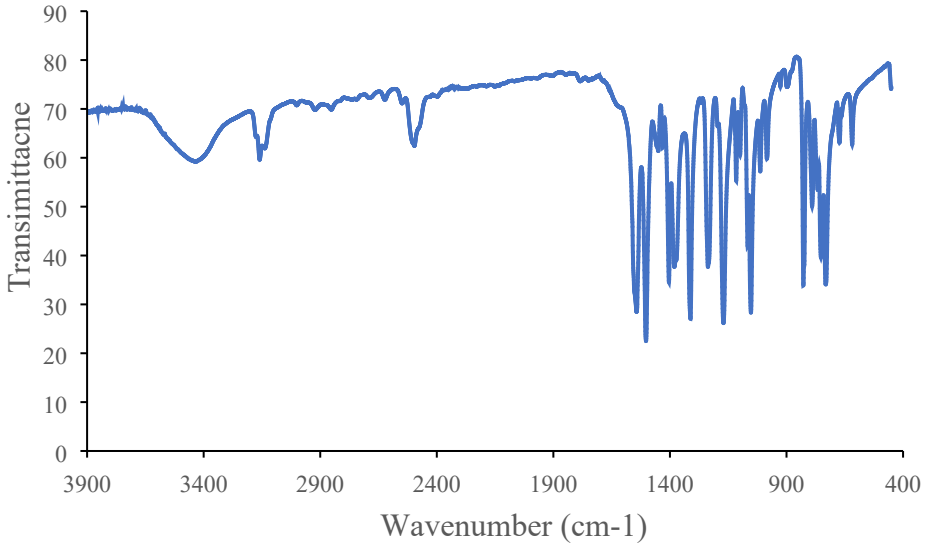

[(Tp)Fe(4-NO_2Tp)]

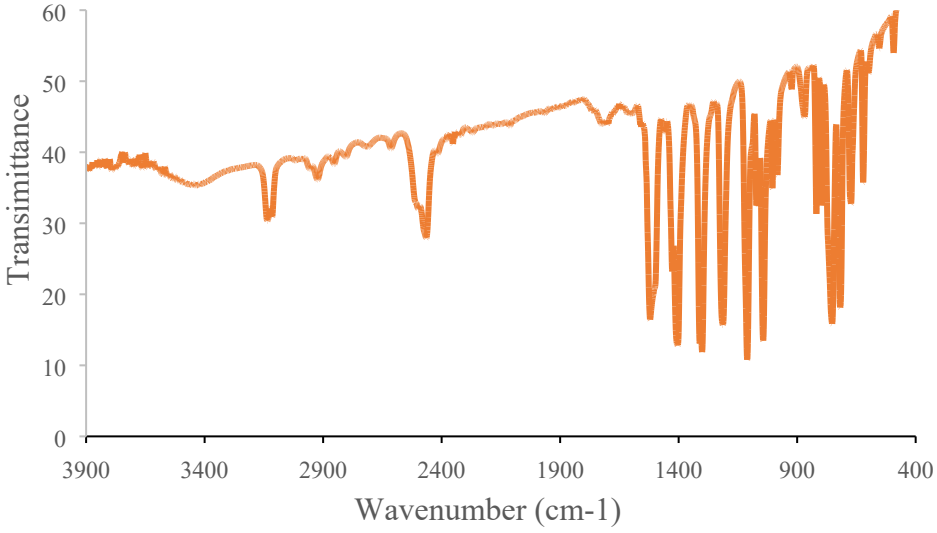

[(Tp)Fe(5-NO_2Tp)]

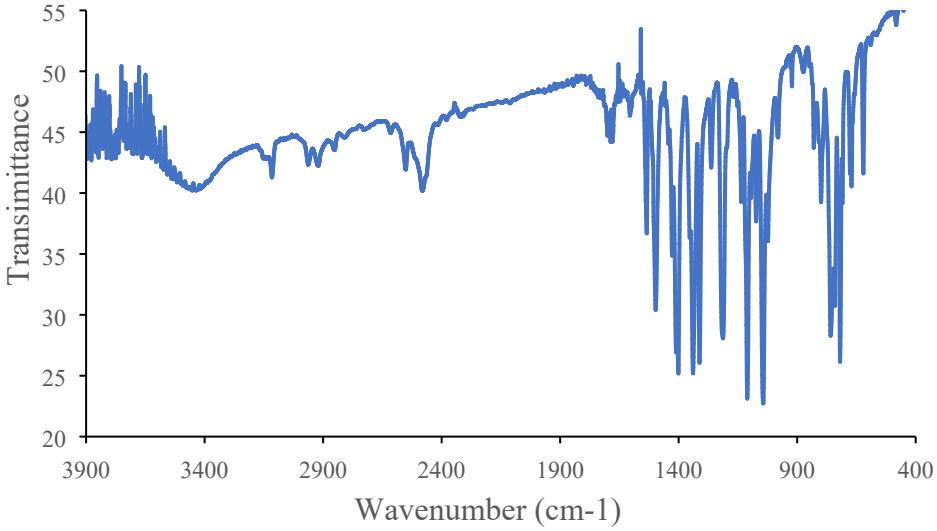

[(3-NH_2Tp)$_2$Fe]

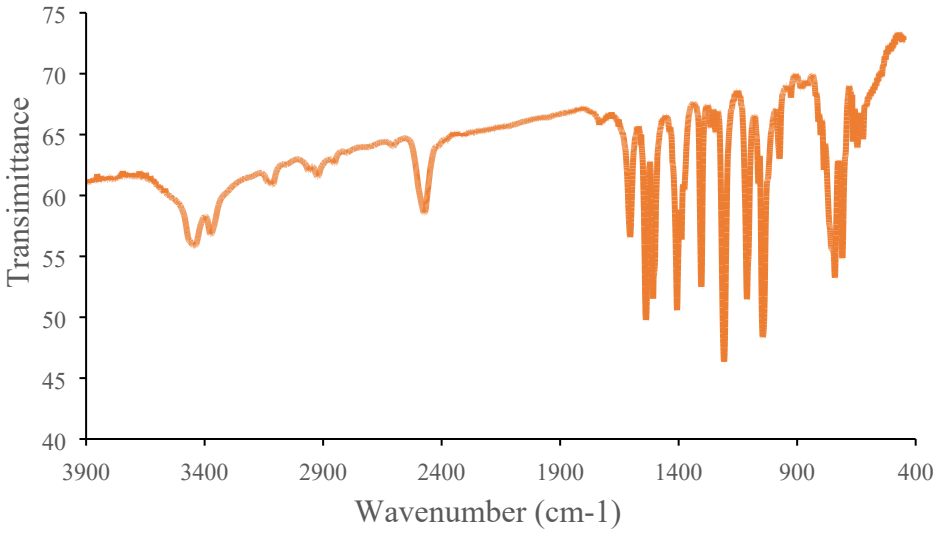

[((3-NH_2)$_2$Tp)$_2$Fe]

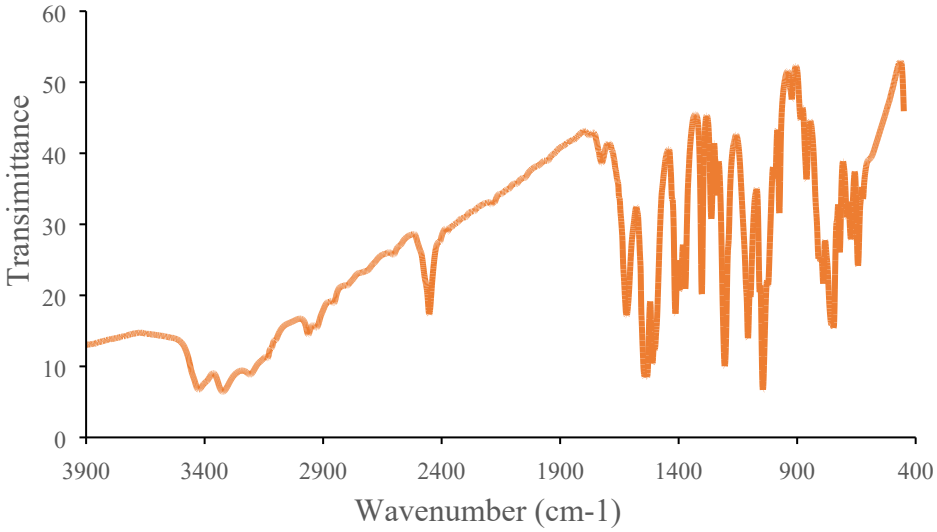
Transimittance
60
50
40
30
20
10
0
3900
3400
2900
2400
1900
1400
900
400
Wavenumber (cm-1)

UV-vis

TBA[3-NO_2Tp] in acetone

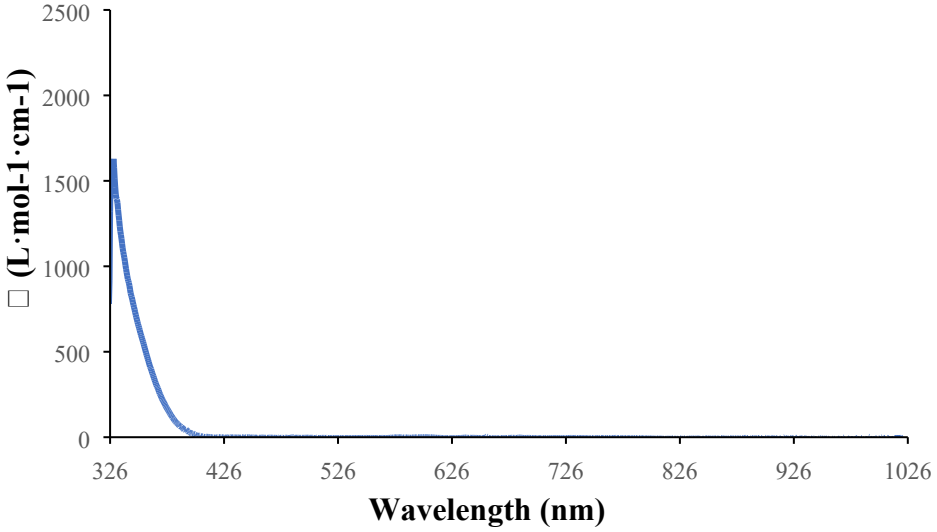

Figure 28. UV-VIS spectrum of TBA[3-NO_2Tp] in acetone.

TBA[(3-NO_2)$_2$Tp] in acetone

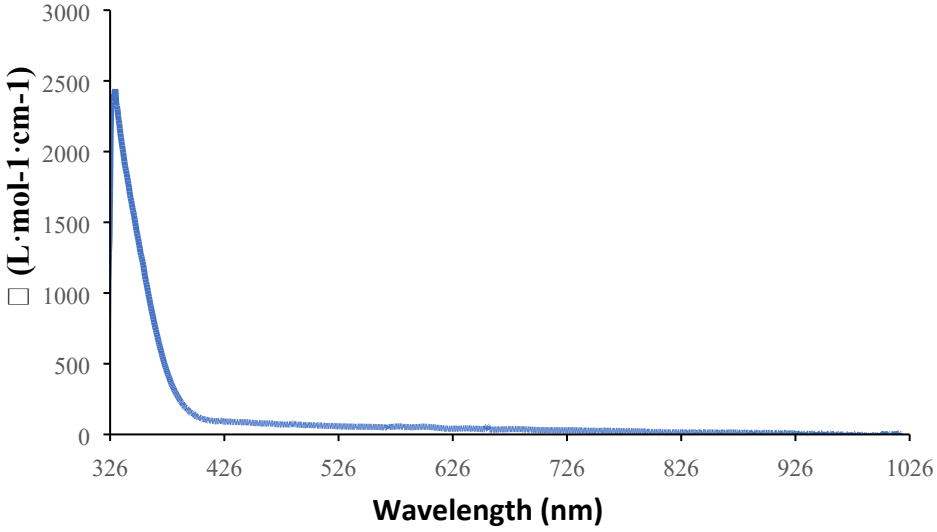

Figure 29. UV-VIS spectrum in TBA[(3-NO_2)$_2$Tp] in acetone.

[(3-NO_2Tp)$_2$Fe] in toluene

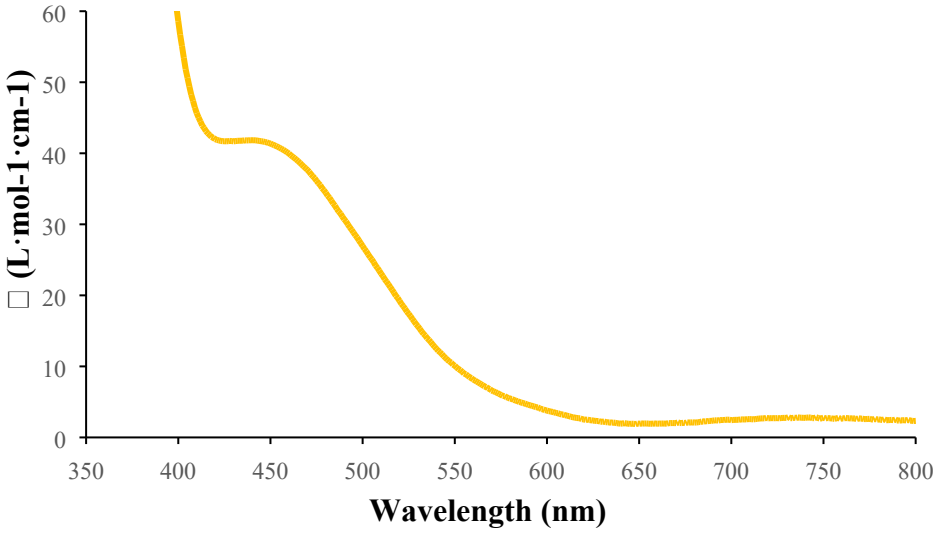

Figure 30. UV-VIS spectrum of [(3-NO_2Tp)$_2$Fe] in toluene.

[(Tp)Fe(3-NO_2Tp)] in toluene

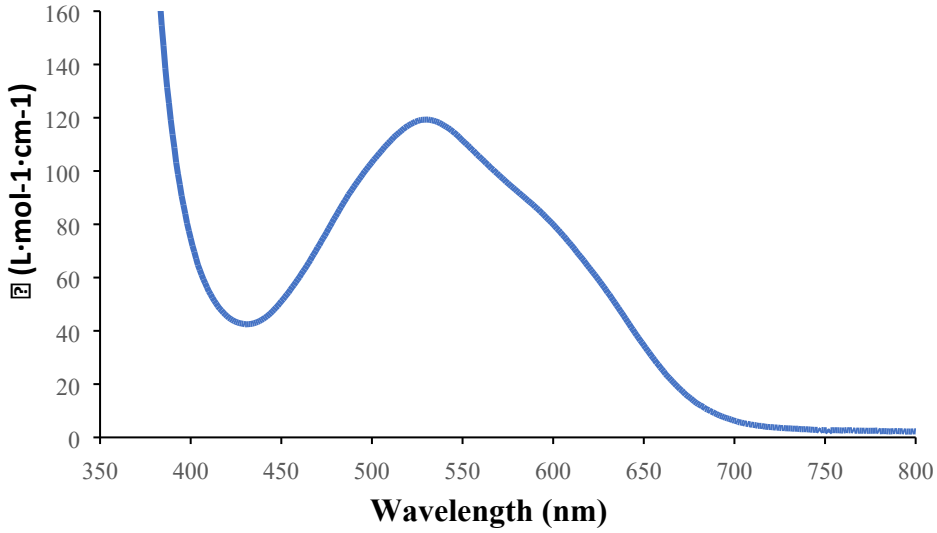

Figure 31. UV-VIS spectrum of [(Tp)Fe(3-NO_2Tp)] in toluene. The absorption band maximum is located at 536 nm.

[((3-NO_2)$_2$Tp)$_2$Fe] in DCM

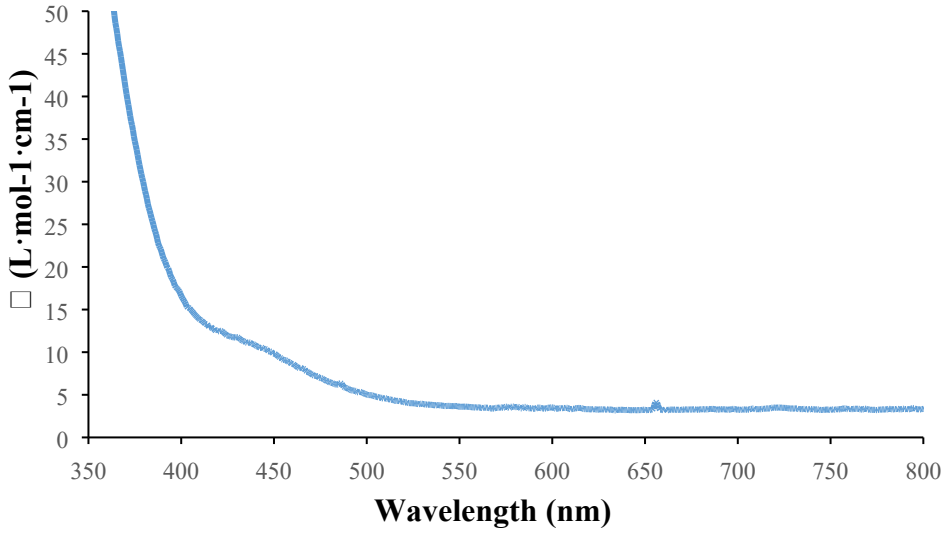

Figure 32. UV-VIS spectrum of [((3-NO_2)$_2$Tp)$_2$Fe] in DCM.

[(Tp)Fe(4-NO_2Tp)] in toluene

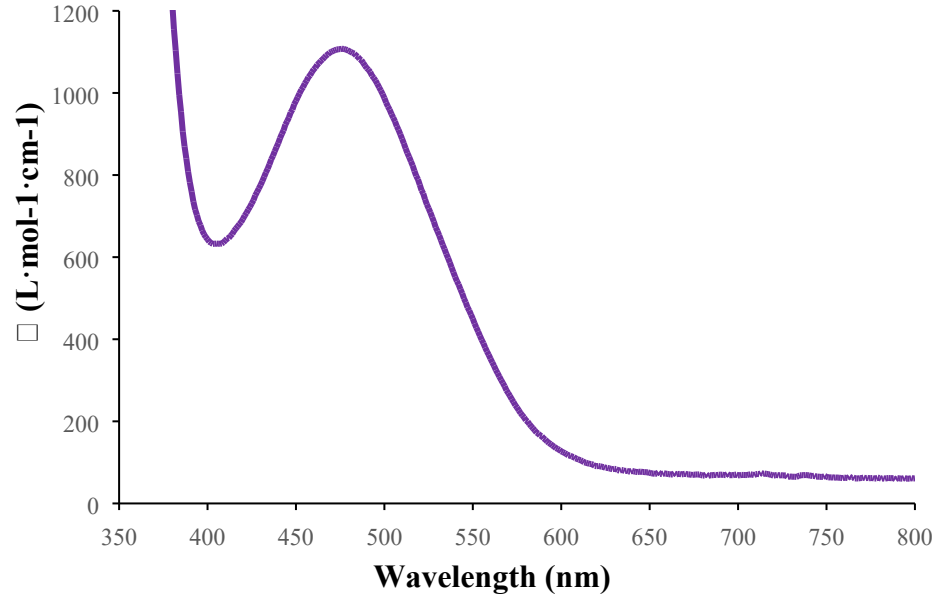

Figure 33. UV-VIS spectrum of [(Tp)Fe(4-NO_2Tp)] in toluene. The absorption band maximum is located at 484 nm.

[(Tp)Fe(5-NO_2Tp)] in toluene

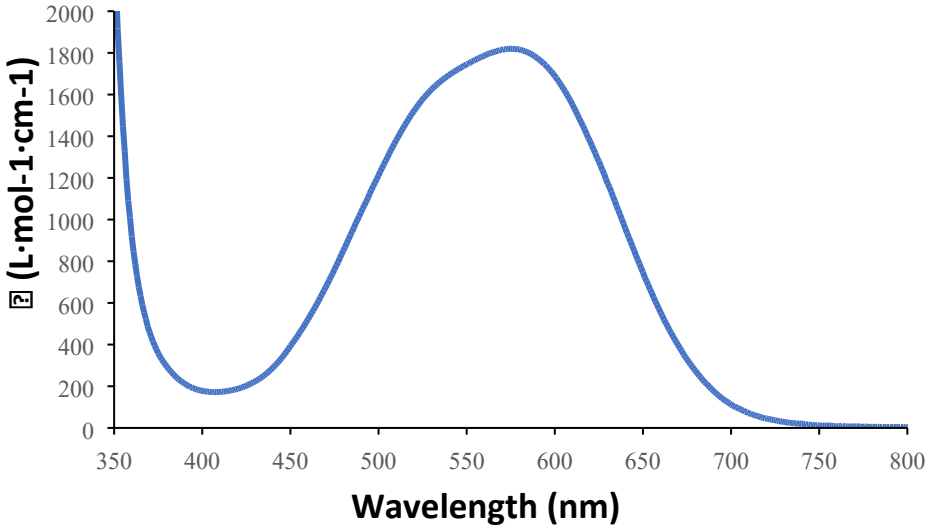

Figure 34. UV-VIS spectrum of [(Tp)Fe(5-NO_2Tp)] in Toluene. The absorption band maximum is located at 585 nm.

[(3-NH_2Tp)$_2$Fe] in DCM

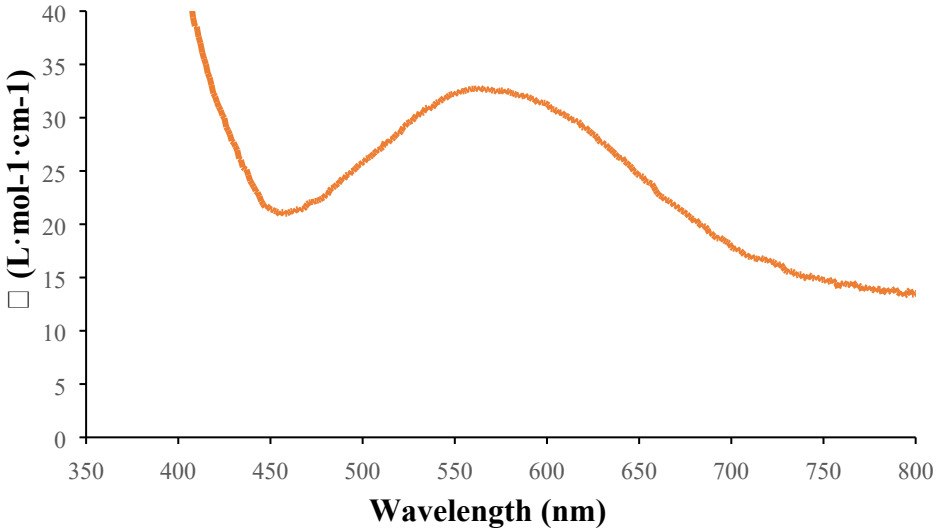

Figure 35. UV-VIS spectrum of [(3-NH_2Tp)$_2$Fe] in toluene. The absorption band maximum is located at 565 nm.

[(3-NH_2)$_2$Tp)$_2$Fe] in DCM

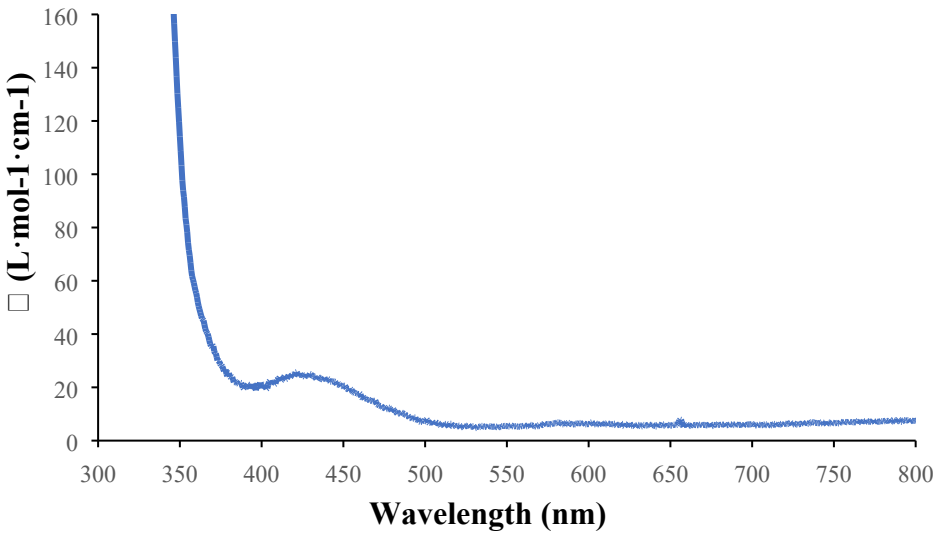

Figure 36. UV-VIS spectrum of $[(3\text{-}NH_2)_2Tp)_2Fe]$ in DCM.

Thermogravimetric analysis

[(3-NO_2Tp)$_2$Fe] in air

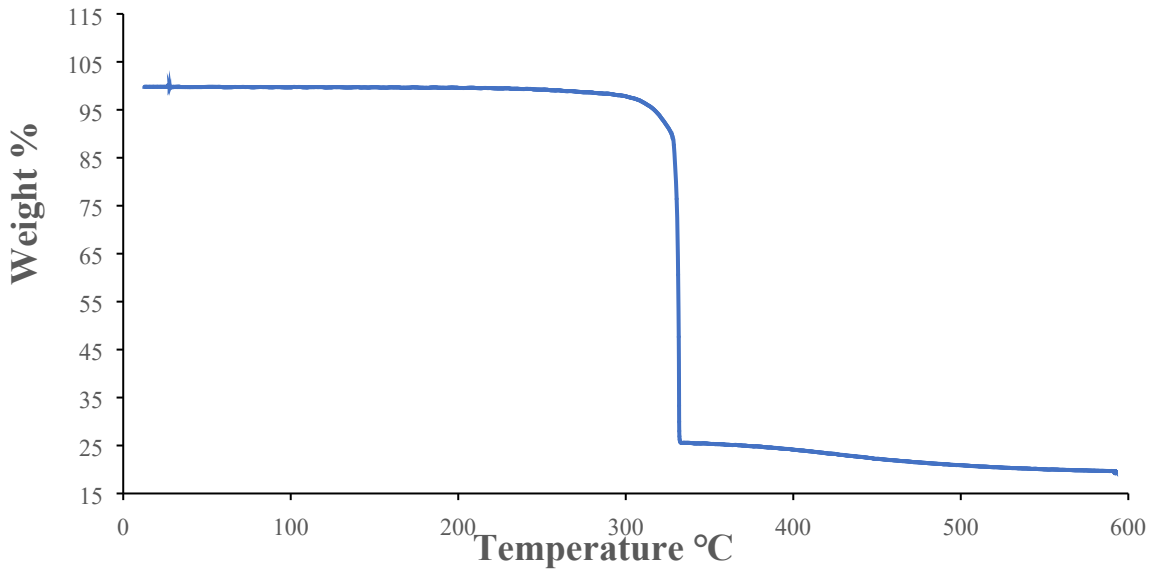

Figure 37. TGA of [(3-NO_2Tp)$_2$Fe] in air

[(Tp)Fe(3-NO_2Tp)] ·0.5 C_6H_6 in air

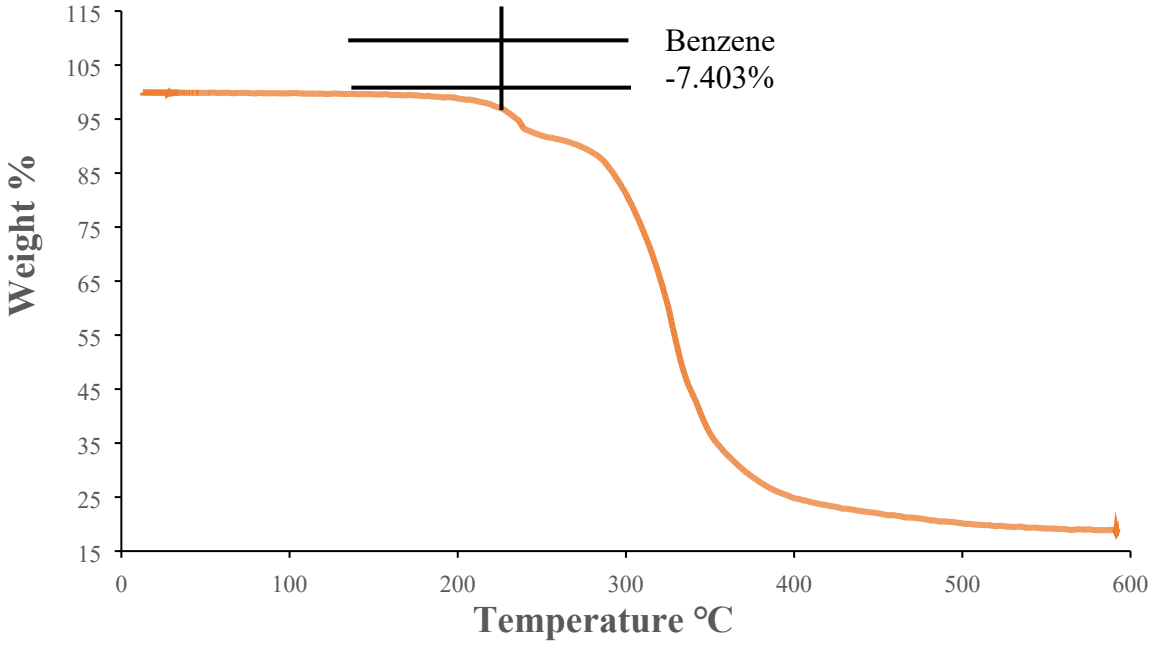

Figure 38. TGA of [(Tp)Fe(3-NO_2Tp)]·0.5 C_6H_6 in air

[((3-NO_2)$_2$Tp)$_2$Fe] in air

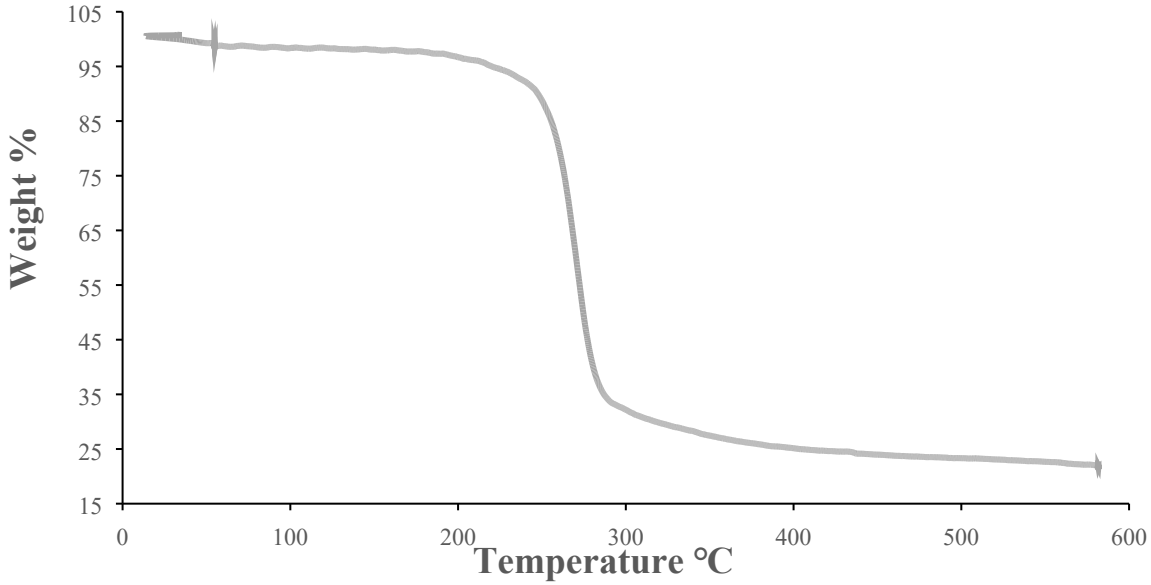

Figure 39. TGA of [((3-NO_2)$_2$Tp)$_2$Fe] in air

[(Tp)Fe(4-NO_2Tp)] in air

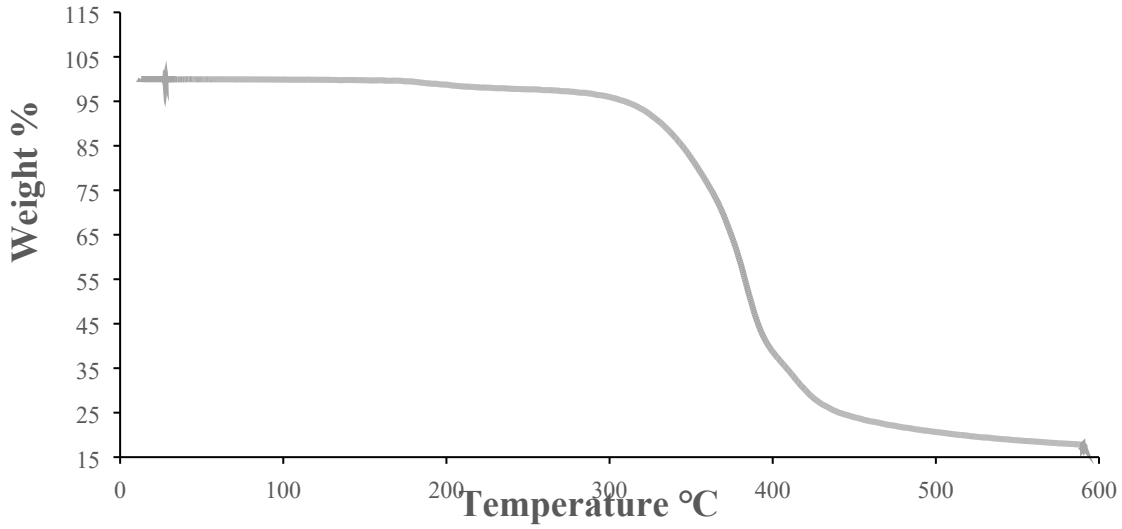

Figure 40. TGA of [(Tp)Fe(4-NO_2Tp)] in air

[(Tp)Fe(5-NO_2Tp)]·0.5 CH_3CN in air

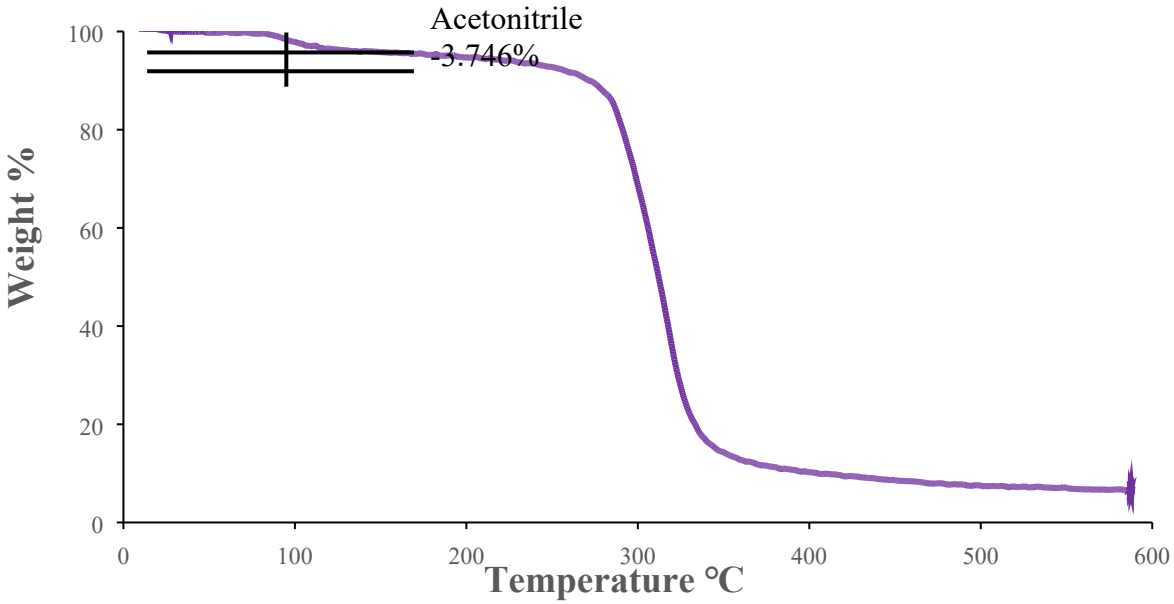

Figure 41. TGA of [(Tp)Fe(5-NO_2Tp)]·0.5 CH_3CN in air

[(3-NH_2Tp)$_2$Fe] in air

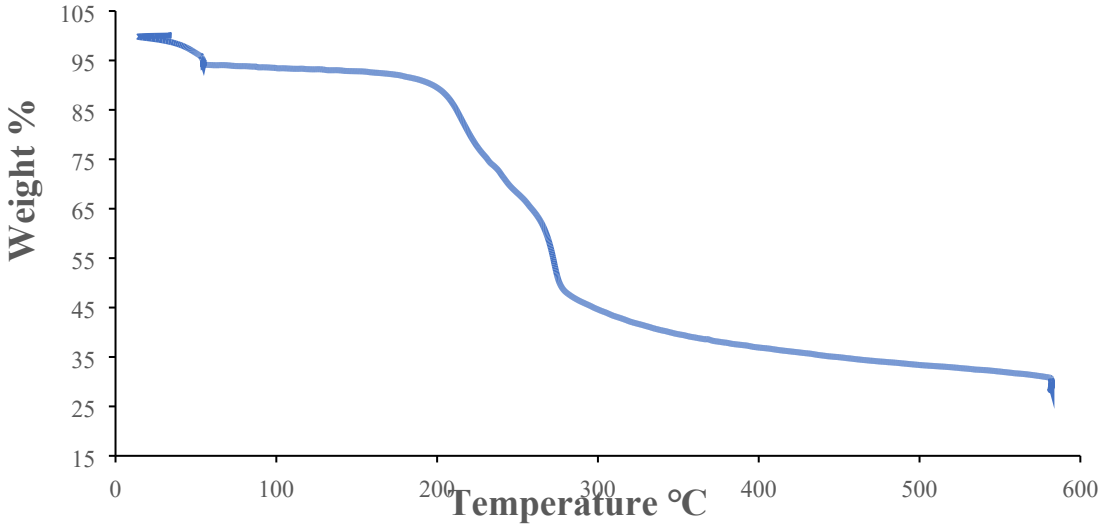

Figure 42. TGA of [(3-NH_2Tp)$_2$Fe] in air

[((3-NH_2)$_2$Tp)$_2$Fe] in air

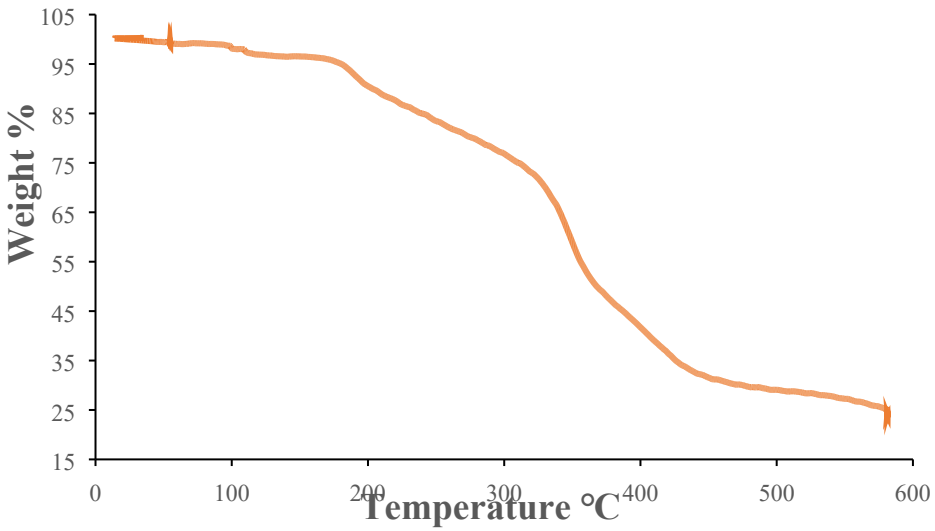

Figure 43. TGA of [((3-NH_2)$_2$Tp)$_2$Fe] in air

SQUID Magnetization data

[(3-NO_2Tp)$_2$Fe]

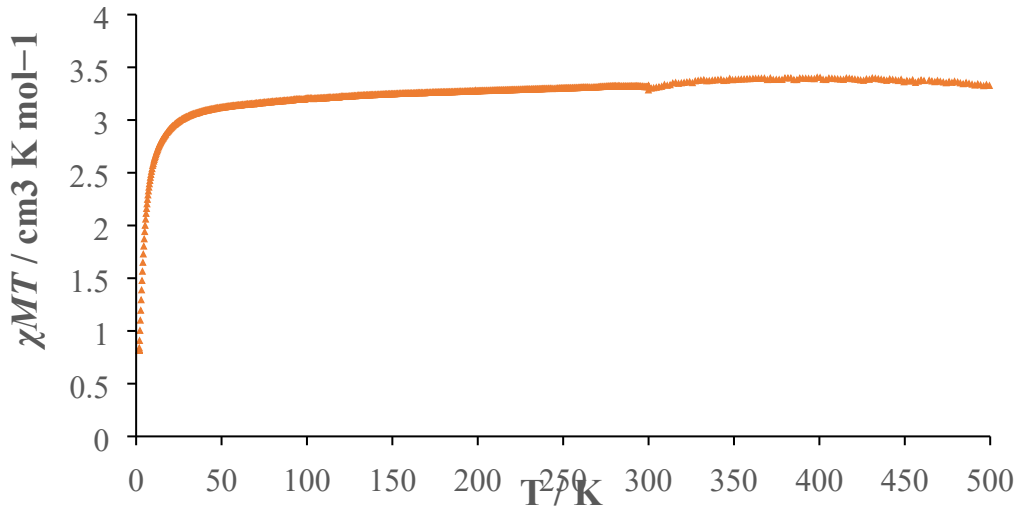

Figure 44. Temperature dependence of the molecular magnetic susceptibility of complexes [(3-NO_2Tp)$_2$Fe] at 0.1 T.

[(Tp)Fe(3-NO_2Tp)]

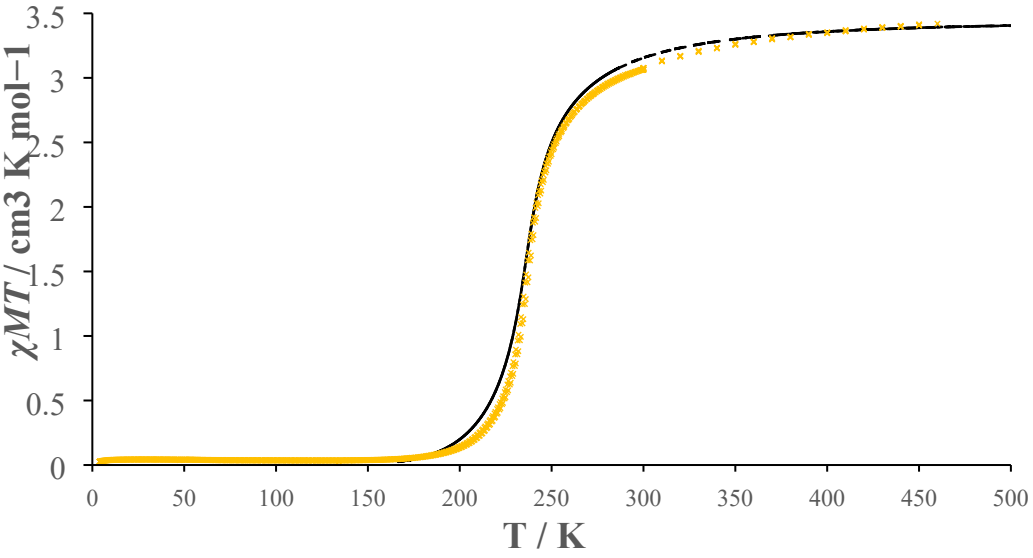

Figure 45. Temperature dependence of the molecular magnetic susceptibility of [(Tp)Fe(3-NO_2Tp)]·$(C_6H_6)_{0.5}$ (x) at 0.1 T with best fits based on the Schlichter-Drickamer model (black dash line).

SCO fit parameters	$T_{1/2}$ / K	$\Delta_r H$ / kJ mol^{-1}	$\Delta_r S$ / J mol^{-1} K^{-1}	Γ / kJ mol^{-1}
	249	13	54.7	2.9

[(Tp)Fe(4-NO_2Tp)]

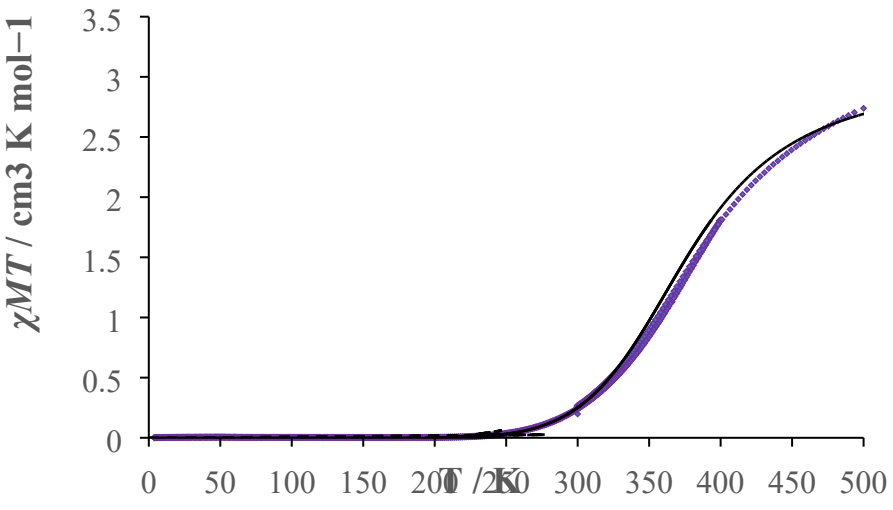

Figure 46. Temperature dependence of the molecular magnetic susceptibility of [(Tp)Fe(4-NO_2Tp)] (◆) at 0.1 T with best fits based on the Schlichter-Drickamer model (black dash line).

SCO fit parameters	$T_{1/2}$ / K	$\Delta_r H$ / kJ mol^{-1}	$\Delta_r S$ / J mol^{-1} K^{-1}	Γ / kJ mol^{-1}
	384	24.4	65	1.2

[(Tp)Fe(5-NO_2Tp)]

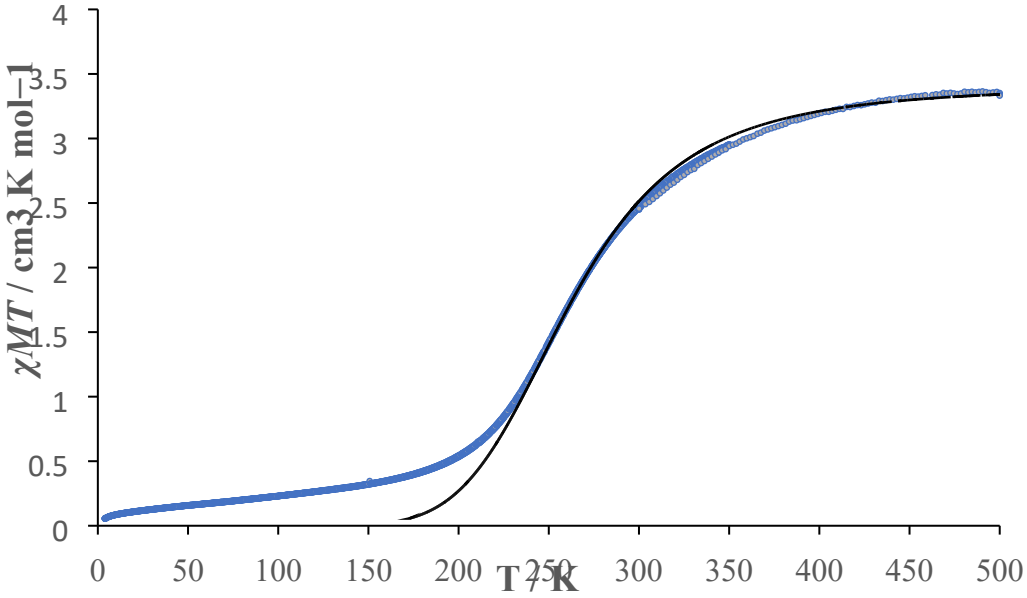

Figure 47. Temperature dependence of the molecular magnetic susceptibility of [(Tp)Fe(5-NO_2Tp)] (●) at 0.1 T with best fits based on the Schlichter-Drickamer model (black dash line).

SCO fit parameters	$T_{1/2}$ / K	$\Delta_r H$ / kJ mol^{-1}	$\Delta_r S$ / J mol^{-1} K^{-1}	Γ / kJ mol^{-1}
	252	17	65	0.1

[(3-NH_2Tp)$_2$Fe]

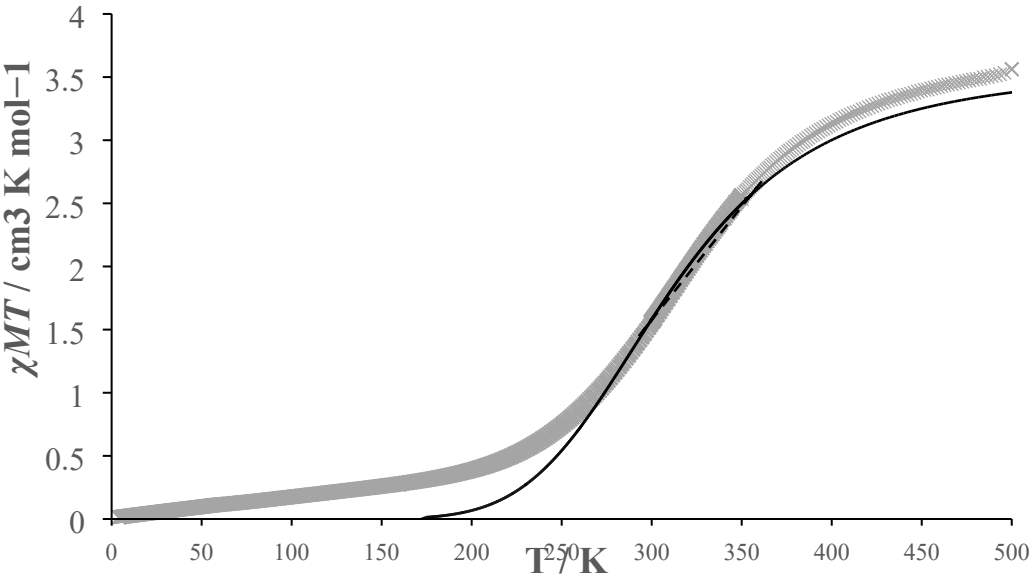

Figure 48. Temperature dependence of the molecular magnetic susceptibility of [(3-NH_2Tp)$_2$Fe] (×) at 0.1 T with best fits based on the Schlichter-Drickamer model (black dash line).

SCO fit parameters	$T_{1/2}$ / K	$\Delta_r H$ / kJ mol^{-1}	$\Delta_r S$ / J mol^{-1} K^{-1}	Γ / kJ mol^{-1}
	316	18.5	59.7	1.0

[((3-NO_2)$_2$Tp)$_2$Fe]

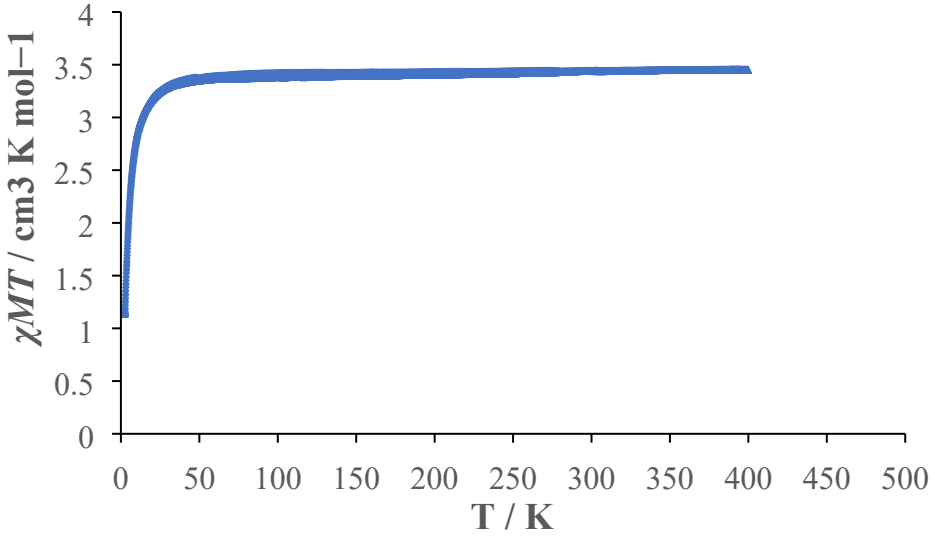

Figure 49. Temperature dependence of the molecular magnetic susceptibility of [((3-NO_2)$_2$Tp)$_2$Fe] at 0.1 T.

[((3-NH_2)$_2$Tp)$_2$Fe]

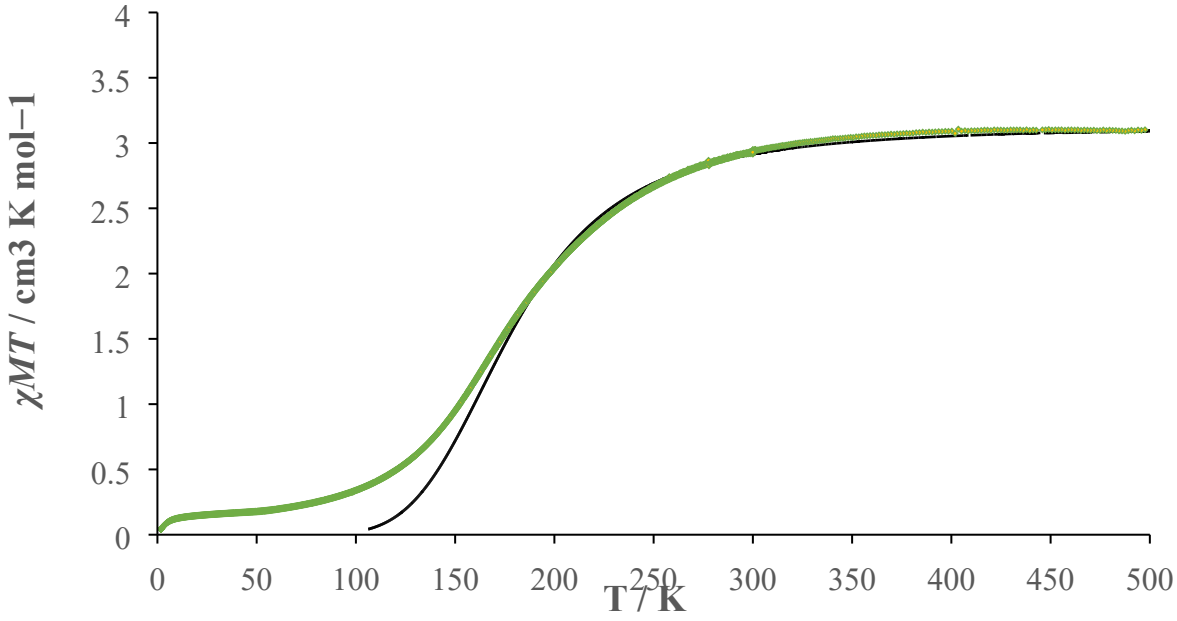

Figure 50. Temperature dependence of the molecular magnetic susceptibility of [((3-NH_2)$_2$Tp)$_2$Fe] (◆) at 0.1 T with best fits based on the Schlichter-Drickamer model (black dash line).

SCO fit parameters	$T_{1/2}$ / K	$\Delta_r H$ / kJ mol^{-1}	$\Delta_r S$ / J mol^{-1} K^{-1}	Γ / kJ mol^{-1}
	178	9.3	52	0

Slichter-Drickamer fitting parameters. Number between parentheses represent 95% confidence interval error bars.

	[(Tp)Fe(3-NO_2Tp)]·(C_6H_6)$_{0.5}$	[(Tp)Fe(4-NO_2Tp)]	[(Tp)Fe(5-NO_2Tp)]	[(3-NH_2Tp)$_2$Fe]	[((3-NH_2)$_2$Tp)$_2$Fe]	[(4-NO_2Tp)$_2$Fe]	[(Tp)Fe((4-NO_2)$_2$Tp)]	[((4-NO_2)$_2$Tp)$_2$Fe]	[(4-NH_2Tp)$_2$Fe]
$\chi_M T_{max}$	3.46	3	3.42	3.62	3.15	3.3	3.3	3	3
$T_{1/2}$ / K	249	384	252	316	178	394	401	456	388
$\Delta_r H$ / kJ mol^{-1}	13 (12.8, 13.2)	24.4 (23.7, 25.2)	17.0 (16.7,17.3)	18.5 (17.9, 19.1)	9.3 (9.2, 9.4)	26.0 (25.4, 26.6)	29.0 (25. 0, 33.0)	34.0 (11.6, 56.4)	19.0 (10.1, 28.0)
$\Delta_r S$ / J mol^{-1}	54.7 (53.9, 55.5)	65.0 (63, 67)	65.0 (63.9,66.1)	59.7 (57.9, 61.6)	52.0 (45.7, 46,4)	65.9 (64.7, 67.0)	72.3 (62.3, 81.8)	74.5 (26.3, 122.6)	50.0 (27.0, 73.0)
Γ / kJ mol^{-1}	2.9 (2.8, 3.1)	1.2 (0.96, 1.48)	0 (0, 0.35)	0 (0, 0.26)	0 (0, 0.08)	6.6 (6.01, 7.57)	4.0 (0.59, 7.40)	0.6 (0, 6.50)	1.3 (0, 4.40)
Number of nearest neighbors in the crystal	9	8	6, 12[a]	6, 12	6	8	8, 11	8	12, 14
Reference	This work	This work	This work	This work	This work	*b*	*b*	*b*	*c*

a: Data given for [(Tp)Fe(5-NO_2Tp)]·(CH_3CN)$_{0.5}$ *b.* Revised fit of the data from reference [1]. *v*. Reference [1].

1. Flototto, H.; Secker, T.; Kogerler, P.; Besson, C., Amine-Functionalized Spin Crossover Building Blocks. *Eur. J. Inorg. Chem.* **2019,** *2019* (43), 4621-4624.